Immunohistochemistry. Paraffin-embedded sections were deparaffinised in xylene and dehydrated through a graded ethanol series. The sections were heated in Tris-EDTA buffer (pH 9.0) for 10 min at 121 °C in an autoclave for antigen retrieval, and endogenous peroxidase was quenched in 0.03% hydrogen peroxidase for 15 min. The specimens were then incubated with the primary antibody: anti-NRP1 (sc-5307, 1:50; Santa Cruz Biotechnology, Santa Cruz, CA, USA) overnight at 4 °C, or anti-CD31 (LS-B1932; LifeSpan BioSciences, Seattle, WA, USA) for 1 h at room temperature. The remaining steps were carried out with the Envision + System-HRP (DAKO, Glostrup, Denmark), followed by counterstaining with haematoxylin. Specificity of this antibody was verified by immunostaining of human kidney tissue samples. To assess tissue NRP1 expression, the sections were scored semi-quantitatively (on a scale of Immunohistochemistry (IHC)-0–3: negative = 0, weak = 1, moderate = 2, and strong = 3) according to the intensity of chromogen deposition in 10% or more of the neoplastic cells.

Microvessel density. Microvessel density (MVD) was measured by counting the number of CD31-positive blood vessels at selected

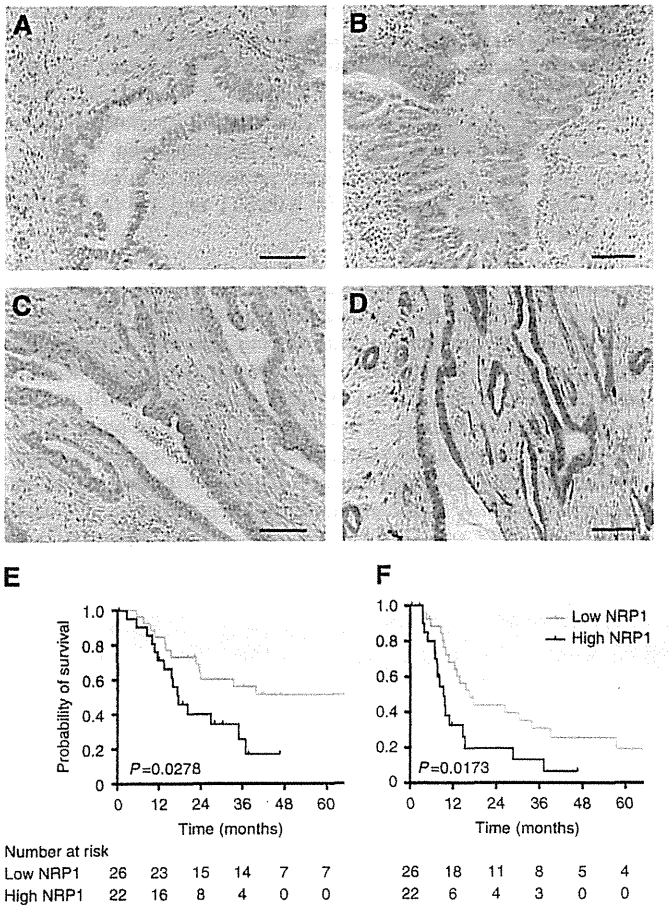

Figure 1. (**A–D**) Representative photomicrographs showing immunohistochemical staining and detailed expression of neuropilin-1 (NRP1, brown colour) in pancreatic ductal adenocarcinomas. Nine (18.8%) cases were negative (IHC-0, **A**), 17 (35.4%) were weakly positive (IHC-1 +, **B**), 12 (25.0%) were moderately positive (IHC-2 +, **C**), and 10 (20.8%) were strongly positive (IHC-3 +, **D**). (**E** and **F**) Kaplan–Meier analysis of overall survival (**E**) and disease-free survival (**F**) in relation to low (IHC-0/1 +) or high (IHC-2 +/3 +) NRP1 expression in pancreatic cancer. Patients with high NRP1 expression showed shorter overall survival ($P = 0.0278$) and disease-free survival ($P = 0.0173$) than patients with low NRP1 expression.

Table 1. Correlation between neuropilin-1 (NRP1) expression and clinicopathological parameters of patients with pancreatic cancer

		NRP1 level			
Characteristics	**All cases**	**Low**	**High**	χ^2	***P*-value**
Total participants	48	26	22		
Age at surgery (years)					
<60	14	8	6	0.003	0.958
⩾60	34	18	16		
Gender					
Male	24	13	11	0.084	0.772
Female	24	13	11		
Tumour grade					
Well	2	1	1	0.031	0.985
Moderately	44	24	20		
Poorly	2	1	1		
Tumour location					
Head	40	23	17	0.420	0.517
Body/Tail	8	3	5		
Tumour size					
<40 mm	29	16	13	0.015	0.902
⩾40 mm	19	10	9		
T factor					
T1/T2	2	2	0	1.812	0.404
T3	16	8	8		
T4	30	16	14		
Lymph-node metastasis					
Positive	35	17	18	0.904	0.342
Negative	13	9	4		
Vascular invasion					
Positive	12	4	8	1.790	0.181
Negative	36	22	14		
Perineural invasion					
Positive	24	11	13	0.755	0.385
Negative	24	15	9		
Microvessel density[a]					
<25	16	13	3	5.549	0.018
⩾25	32	13	19		
Resection margin					
Positive	13	7	6	0.089	0.765
Negative	35	19	16		
CEA					
Normal	20	13	7	0.959	0.327
High	28	13	15		
CA19-9					
Normal	16	12	4	3.032	0.082
High	32	14	18		

Abbreviation: CEA=carcinoembryonic antigen.
[a]Number of vessels per 100 magnification field.

hotspots in high-magnification fields (× 200). Four randomly selected regions were analysed and averaged.

Statistical analysis. Values are presented as the means and standard deviation. Statistical analyses were conducted using Dr SPSS II for Windows software (SPSS Inc., Chicago, IL, USA). Differences between groups were assessed statistically using Student's *t*-test or Tukey–Kramer test for parametric data, or the Mann–Whitney *U*-test for non-parametric data. Overall and disease-free survival curves were drawn according to the Kaplan–Meier method, and differences between the curves were analysed by applying the log-rank test. Multivariate Cox regression analysis was used to analyse the independent prognostic factors related to survival. Differences at $P<0.05$ were considered to be statistically significant.

RESULTS

Correlation of NRP1 overexpression with poor outcome in clinical cases of pancreatic cancer. Neuropilin-1 immunostaining in clinical specimens of pancreatic ductal adenocarcinoma from 48 patients was predominantly identified in the cytoplasm and on the cell surfaces of malignant ductal cells (Figure 1). According to the semi-quantitative assessment criteria employed, the specimens were divided into 4 groups: 9 cases (19.7%) that were negative (IHC-0, Figure 1A), 17 (35.4%) that were weakly immunostained (IHC-1+, Figure 1B), 12 (25.0%) that were moderately immunostained (IHC-2+, Figure 1C), and 10 (20.8%) that showed strongly positive immunostaining (IHC-3+, Figure 1D). Comparisons between low NRP1 expression (IHC-0/1+) and high NRP1 expression (IHC-2+/3+) demonstrated similar clinicopathological features, except for MVD within the tumour ($P=0.018$, Table 1). The 3- and 5-year survival rates for the 48 patients overall were 54.2% and 12.5%, respectively. Kaplan–Meier analysis demonstrated a significant difference in overall survival between the groups showing high NRP1 expression (median 16.7 months, range 0.5–46.6 months) and low NRP1 expression (median 34.9 months, range 5.6–94.3 months) ($P=0.0278$, Figure 1E). Disease-free survival also differed significantly between high (median 8.2 months, range 0.5–46.6 months) and low NRP1 expression (median 16.1 months, range 3.2–94.3 months) ($P=0.017$, Figure 1F). Multivariate analysis using the Cox proportional hazards model indicated that, apart from positivity for lymph-node metastasis (hazard ratio (HR) = 5.620, 95% confidence interval (CI): 1.312–24.071, $P=0.020$), involvement of the resection margin (HR = 5.394, 95% CI: 2.227–13.068, $P<0.001$) and high expression of NRP1 (HR = 2.391, 95% CI: 1.045–5.469, $P=0.039$) were significantly correlated with poor overall survival, and were independent prognostic factors for pancreatic cancer (Table 2).

iRGD peptide facilitates drug penetration into murine pancreatic cancer models showing NRP1 overexpression. To investigate the activity of iRGD peptide, co-injection of Evans blue dye, and fluorochrome-labelled dextran was performed. Evans blue dye accumulation was enhanced 1.9-fold in two CXs (BxPC-3 and MIA PaCa-2) by co-administration of iRGD; however, enhanced dye accumulation was not observed in the remaining three CXs (Figure 2A; Supplementary Figure S1).

To evaluate the correlation between the iRGD inducing drug penetration effect and NRP1 expression in cancer cells, IHC was performed. Two CXs that showed enhanced dye accumulation were strongly positive (3+), and the remaining three CXs were weakly positive (1+) (Figure 2B; Supplementary Figure S2).

Three CXs (BxPC-3, MIA PaCa-2, and SUIT-2) and three TGs that showed NRP1 overexpression (Supplementary Figure S2) were employed in dextran experiments. Co-administration of iRGD peptide induced the dextran penetration into tumour parenchyma compared with dextran single administration (Figures 2C and D). Extended dextran-positive areas in CXs were 1.8-fold in BxPC-3 ($P=0.001$) and 2.1-fold in MIA PaCa-2 ($P=0.024$), but had no effect in SUIT-2 (Figure 2E). Penetration of dextran by co-administration of iRGD peptide was also observed in TGs, the areas of dextran distribution were extended 1.7-fold in PC-03 ($P=0.008$), 3.0-fold in PC-09 ($P=0.001$), and 1.9-fold in PC-10 ($P=0.040$) (Figure 2E).

Enhancement of the anticancer effect by co-administration of GEM and iRGD peptide in comparison with GEM monotherapy. Enhanced drug penetration into tumour was evaluated by Evans blue dye as a drug substitute tracer (Figure 3A). Drug accumulations in two CXs and one TG (PC-03) were significantly enhanced by iRGD co-administration; however, the effects in other two TGs (PC-09 and 10) were not remarkable. Similarly, co-administration of iRGD with GEM significantly decreased tumour growth in comparison with GEM monotherapy in BxPC-3 ($P=0.046$, Figures 3B and C) and MIA PaCa-2 ($P=0.037$, Figure 3C). One TG model (PC-03) also showed a significant tumour growth

Table 2. Cox proportinal hazards model of prognostic factors in patients with pancreatic cancer ($n=48$)

	Univariate analysis			Multivariate analysis		
Factor	HR	95% CI	*P*-value	HR	95% CI	*P*-value
Age (⩾60 years)	0.934	0.418–2.084	0.867	NA	NA	NA
Gender (male)	0.885	0.415–1.887	0.752	NA	NA	NA
T factor (T4)	1.433	0.642–3.199	0.380	NA	NA	NA
Tumour size (⩾40 mm)	2.166	1.010–4.646	0.047	1.738	0.748–4.042	0.199
Lymph-node status (positive)	6.712	1.585–28.421	0.010	5.620	1.312–24.071	0.020
Vascular invasion (positive)	1.768	0.769–4.068	0.180	NA	NA	NA
Perineural invasion (positive)	1.726	0.797–3.740	0.166	NA	NA	NA
Resection margin (positive)	5.757	2.501–13.251	<0.001	5.394	2.227–13.068	<0.001
Microvessel density[a] (⩾25)	1.214	0.543–2.715	0.637	NA	NA	NA
Neuropilin-1 expression (high)	2.334	1.072–5.083	0.033	2.391	1.045–5.469	0.039

Abbreviations: CI = confidence interval; HR = hazard ratio; NA = not applicable.
[a]Number of vessels per 100 magnification field.

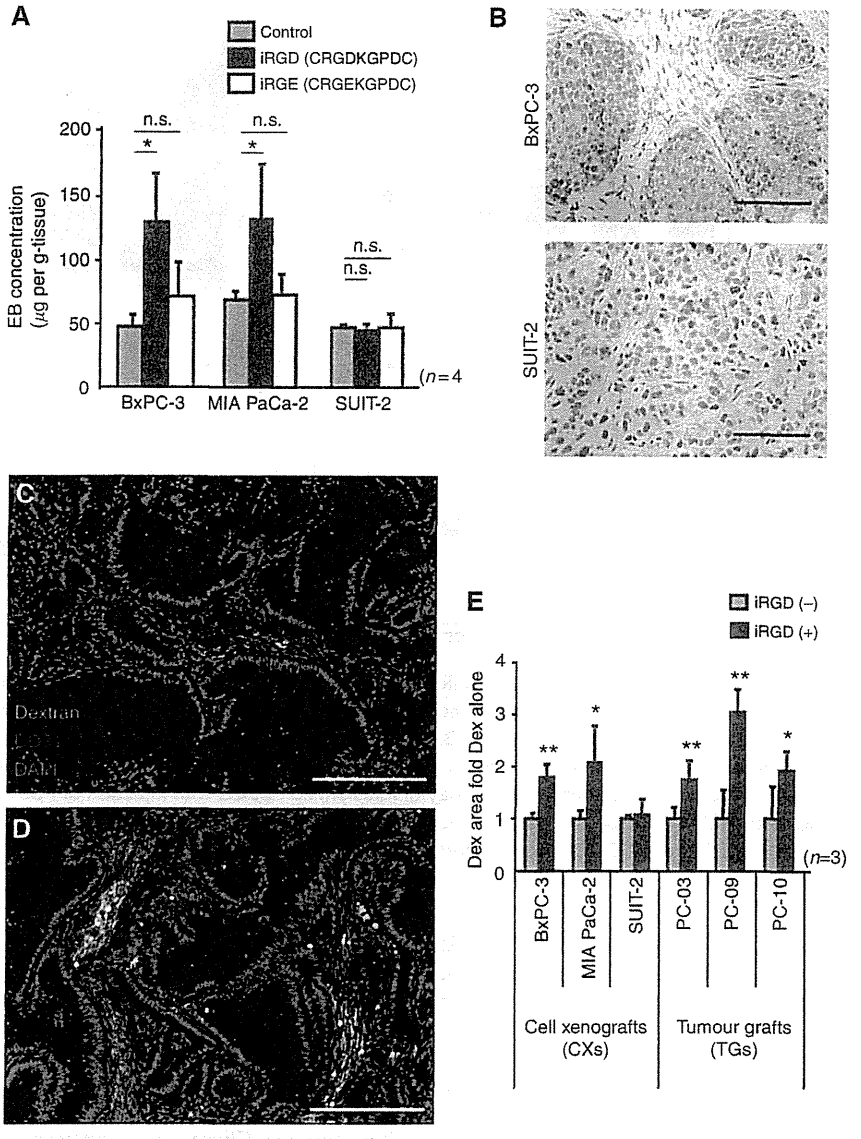

Figure 2. (**A**) Evans blue dye accumulation assay for cell line-based xenograft models (cell xenografts: CXs). Co-administration of iRGD peptide with a drug (black bar) was compared with administration of a single drug alone (grey bar) or iRGE peptide (white bar). Dye accumulation was enhanced 1.9-fold in BxPC-3 and MIA PaCa-2, but not in SUIT-2. Control peptide (iRGE) showed no enhancement of dye accumulation ($N=4$ per group). (**B**) Neuropilin-1 (NRP1) expression in animal models (× 400 magnification; scale bar, 100 μm). Overexpression of NRP1 was shown in BxPC-3 (upper) and MIA PaCa-2 (not shown), but not in SUIT-2 (lower). (**C** and **D**) Distribution of fluorochrome (Alexa-488, green)-labelled dextran in frozen sections of PC-09 (× 200 magnification; scale bar, 200 μm). Tumour vasculature was stained with anti-CD31 antibody (red), and nuclei were stained with DAPI (blue). Dextran appeared faintly after single administration (**C**), and it was more widely distributed with a stronger intensity after co-administration with iRGD peptide (**D**). (**E**) The areas of dextran distribution were calculated and compared. iRGD co-administration increased the area of dextran distribution 1.8-fold in BxPC-3 ($P=0.001$), 2.1-fold in MIA PaCa-2 ($P=0.024$), 1.7-fold in PC-03 ($P=0.008$), 3.0-fold in PC-09 ($P=0.001$), and 1.9-fold in PC-10 ($P=0.040$). *$P<0.05$, **$P<0.01$.

suppression by the combination therapy ($P=0.048$), but the other two TGs (PC-09 and 10) exhibited no significant differences (Figure 3C). The body weight of mice was decreased on days 12 and 15 in the GEM administered groups relative to the control group, but there was no significant difference in body weight between the iRGD co-administration group and the GEM monotherapy group (data not shown).

DISCUSSION

The present study conducted to re-evaluate the use of iRGD peptide demonstrated that it boosted the accumulation of drugs in two of five pancreatic cancer CXs that showed high expression of NRP1, and the anticancer effects of GEM were also enhanced by iRGD co-administration in these two CXs. We concluded that iRGD co-administration therapy would be indicated for nearly half of all patients with pancreatic cancer showing NRP1 overexpression, and we further evaluated this possibility using clinically relevant murine pancreatic cancer TG models. Enhancement of drug accumulation by iRGD was also observed in TGs, but the effects were less marked than those in CXs. Additionally, a significant anticancer booster effect of GEM plus iRGD combination therapy was observed in only one model.

First, our experiments using five CXs reconfirmed the enhanced drug accumulation effect of iRGD peptide. It was noteworthy that our experiments demonstrated that the effect of iRGD was dependent on the level of NRP1 expression; that is, the effects of iRGD were marked in two high-NRP1 CXs, but not significant in

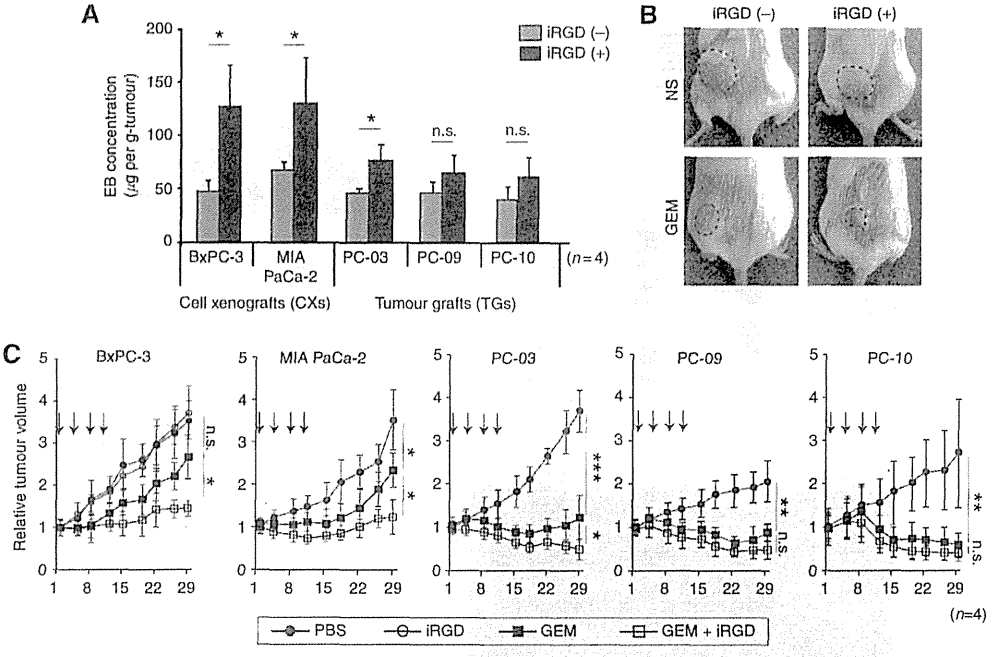

Figure 3. Tumour treatment studies involving co-administration of iRGD peptide. (**A**) Enhanced drug accumulation into tumour using Evans blue dye as a drug substitute tracer. Drug accumulations were enhanced about twofolds by iRGD in two CXs and one TG; however, the effects were not significant in another two TGs. (**B**) Tumour appearances in ectopic BxPC3 models at 28 days after the treatment initiation. (**C**) Tumour growth curves of gemcitabine (GEM) and iRGD combination therapy. Tumour-bearing mice were injected with 100 mg kg^{-1} gemcitabine or 100 μl of PBS (twice per week for 2 weeks; days 1, 4, 8, and 11; arrows show the day of infusion) combined with injection of PBS (Control, and GEM groups) or 8 μmol kg^{-1} iRGD peptide (iRGD, and GEM + iRGD group) 10 min beforehand ($N=4$ per group). Tumour growth curves of two CXs (BxPC-3 and MIA PaCa-2) and three TGs (PC-03, PC-09, and PC-10) are indicated. *$P<0.05$, **$P<0.01$, ***$P<0.001$; n.s., not statistically significant.

three low-NRP1 models. These results suggest that iRGD peptide co-administration would be beneficial for subset patients with NRP1-overexpressing tumours, similarly to a molecular targeting agent.

We then evaluated the populations of pancreatic cancer overexpressing NRP1 in clinical specimens. Neuropilin-1 overexpression was seen in 45.8% of specimens, and the patients concerned had worse outcomes than patients whose tumours had low NRP1 expression (Figures 1E and F). Neuropilin-1 is known to be a co-receptor that enhances the binding of VEGF-A to the VEGF receptor (Soker *et al*, 1998), and NRP1 overexpression induces upregulation of VEGF signalling that is associated with angiogenesis and cancer metastases (Poon *et al*, 2001). Our finding that NRP1 overexpression was associated with higher MVD (Table 1) was considered to reflect upregulation of VEGF signalling. However, it should also be noted that resistance to GEM might have contributed to the differences in outcome. Neuropilin-1-overexpressing pancreatic cancer cell lines showed chemoresistance to GEM *in vitro* (Wey *et al*, 2005). All of the patients included in our study had received GEM-based adjuvant chemotherapy, and the effects of drug resistance should therefore be considered.

The effect of iRGD peptide in enhancing drug penetration is expected to improve the efficacy of treatment for dismal solid tumours, including pancreatic cancer. However, CXs do not adequately represent the clinical features of pancreatic cancer. We therefore employed pancreatic TGs, which have been reported to show better clinical predictive ability (Dong *et al*, 2010; Hidalgo *et al*, 2011; Morelli *et al*, 2012), and our previous evaluation had indicated that the drug delivery characteristics of TGs were more clinically reproducible. Histological findings of pancreatic TGs were more similar to clinical pancreatic cancer compared with CXs, as showing the atypical cancer glands and stromal tissues (Supplementary Figure S2). Internalised-RGD peptide certainly induced drug penetration in all TGs that were overexpressed NRP1, combination therapy using iRGD peptide was considered to be applicable for clinical pancreatic cancer.

Finally, the efficacy of iRGD peptide co-administration with GEM was verified using five pancreatic cancer models that showed enhanced drug accumulation in dextran experiments. In three models, iRGD peptide significantly enhanced drug accumulation into tumour (Figure 3A). Anticancer effect of GEM was also enhanced by iRGD co-administration in these three models (Figure 3C). Therefore, it seems possible to co-administer GEM, which is a key first-line drug for pancreatic cancer, with iRGD peptide, though the molecular size of GEM (0.3 kDa) is smaller than that of agents previously validated (0.6 kDa–130 nm, Sugahara *et al*, 2010). On the other hand, enhanced drug accumulations by iRGD peptide in the remaining two TGs were limited (Figure 3A), and the anticancer effects were also not significantly enhanced (Figure 3C). A major factor influencing the results was considered to be different histological findings among these models. Drug penetrations around the perfusing tumour vessels were not so different between CXs and TGs as shown in dextran experiments (Figure 2E). However, TGs included relative fewer blood vessels and more stromal tissues like clinical pancreatic cancer, as we previously reported (Akashi *et al*, 2013). We therefore considered that the efficacy of iRGD co-administration might be limited in clinical pancreatic cancer, characterised as poor vascularity and prominent desmoplastic reaction. A TG model (PC-03) that showed significant effect of iRGD peptide was established by transplantation of liver metastatic cancer tissue, whereas the other two TGs (PC-09 and 10) were established from primary pancreatic cancer. Histological findings of PC-03 (Supplementary Figure S2) were relatively similar to CXs, as characterised as hypervascular and fewer stromal tissues (Supplementary Figure S2; Akashi *et al*, 2013). Paradoxically, it is presumed that the impact of histological features on the iRGD efficacy is greater. Though, the difference of

drug susceptibility between CXs and TGs should be accounted for the interpretation of our results. As shown in Figure 3C, GEM monotherapy showed <50% inhibition of tumour growth in two CXs. In contrast, tumour growths in both TGs were significantly supressed by GEM monotherapy. Therefore, further validations, such as experiments using GEM-resistant TGs, might be required.

Our re-evaluations of iRGD peptide demonstrated a substantial booster accumulation effect of drugs in mouse pancreatic cancer models with high NRP1 expression, and this effect may be exploitable in nearly half of all patients with pancreatic cancer showing high NRP1 expression. Since the booster anticancer effects of iRGD co-administration with GEM were marked only in cell line-based models but not so great in TGs, the possible clinical application of iRGD peptide should be considered carefully.

ACKNOWLEDGEMENTS

We thank Kazuki N Sugahara, Erkki Ruoslahti, and the members of the Cancer Centre at Sanford-Burnham Medical Research Institute, La Jolla for providing the samples of their peptide. This study was supported by a Grant-in-Aid for Scientific Research (KAKENHI, 23300362 and 23659635) from The Ministry of Education, Culture, Sports, Science, and Technology of Japan.

CONFLICT OF INTEREST

The authors declare no conflict of interest.

REFERENCES

Akashi Y, Oda T, Ohara Y, Miyamoto R, Hashimoto S, Enomoto T, Yamada K, Kobayashi A, Fukunaga K, Ohkochi N (2013) Histological advantages of the tumor graft, a murine model involving transplantation of human pancreatic cancer tissue fragments. *Pancreas* **42**: 1275–1282.

Burris 3rd HA, Moore MJ, Andersen J, Green MR, Rothenberg ML, Modiano MR, Cripps MC, Portenoy RK, Storniolo AM, Tarassoff P, Nelson R, Dorr FA, Stephens CD, Von Hoff DD (1997) Improvements in survival and clinical benefit with gemcitabine as first-line therapy for patients with advanced pancreas cancer: a randomized trial. *J Clin Oncol* **15**: 2403–2413.

Dong X, Guan J, English JC, Flint J, Yee J, Evans K, Murray N, Macaulay C, Ng RT, Gout PW, Lam WL, Laskin J, Ling V, Lam S, Wang Y (2010) Patient-derived first generation xenografts of non-small cell lung cancers: promising tools for predicting drug responses for personalized chemotherapy. *Clin Cancer Res* **16**: 1442–1451.

Fukahi K, Fukasawa M, Neufeld G, Itakura J, Korc M (2004) Aberrant expression of neuropilin-1 and -2 in human pancreatic cancer cells. *Clin Cancer Res* **10**: 581–590.

Hansel DE, Wilentz RE, Yeo CJ, Schulick RD, Montgomery E, Maitra A (2004) Expression of neuropilin-1 in high-grade dysplasia, invasive cancer, and metastases of the human gastrointestinal tract. *Am J Surg Pathol* **28**: 347–356.

Heldin CH, Rubin K, Pietras K, Ostman A (2004) High interstitial fluid pressure - an obstacle in cancer therapy. *Nat Rev Cancer* **4**: 806–813.

Hidalgo M, Bruckheimer E, Rajeshkumar NV, Garrido-Laguna I, De Oliveira E, Rubio-Viqueira B, Strawn S, Wick MJ, Martell J, Sidransky D (2011) A pilot clinical study of treatment guided by personalized tumorgrafts in patients with advanced cancer. *Mol Cancer Ther* **10**: 1311–1316.

Jain RK (1999) Transport of molecules, particles, and cell in solid tumors. *Annu Rev Biomed Eng* **1**: 241–263.

Kolodkin AL, Levengood DV, Rowe EG, Tai YT, Giger RJ, Ginty DD (1997) Neuropilin is a semaphorin III receptor. *Cell* **90**: 753–762.

Li M, Yang H, Chai H, Fisher WE, Wang X, Brunicardi FC, Yao Q, Chen C (2004) Pancreatic carcinoma cells express neuropilins and vascular endothelial growth factor, but not vascular endothelial growth factor receptors. *Cancer* **101**: 2341–2350.

Morelli MP, Calvo E, Ordoñez E, Wick MJ, Viqueira BR, Lopez-Casas PP, Bruckheimer E, Calles-Blanco A, Sidransky D, Hidalgo M (2012) Prioritizing phase I treatment options through preclinical testing on personalized tumorgraft. *J Clin Oncol* **30**: e45–e48.

Müller MW, Giese NA, Swiercz JM, Ceyhan GO, Esposito I, Hinz U, Büchler P, Giese T, Büchler MW, Offermanns S, Friess H (2007) Association of axon guidance factor semaphorin 3A with poor outcome in pancreatic cancer. *Int J Cancer* **121**: 2421–2433.

Parikh AA, Liu WB, Fan F, Stoeltzing O, Reinmuth N, Bruns CJ, Bucana CD, Evans DB, Ellis LM (2003) Expression and regulation of the novel vascular endothelial growth factor receptor neuropilin-1 by epidermal growth factor in human pancreatic carcinoma. *Cancer* **98**: 720–729.

Poon RT, Fan ST, Wong J (2001) Clinical implications of circulating angiogenic growth factors in cancer patients. *J Clin Oncol* **19**: 1207–1225.

Ruoslahti E, Bhatia SN, Sailor MJ (2010) Targeting of drugs and nanoparticles to tumors. *J Cell Biol* **188**: 759–768.

Sobin LH, Gospodarowicz MK, Wittekind C (2009) *TNM Classification of Malignant Tumours*. 7th edn. Wiley-Blackwell: Chichester, UK.

Soker S, Fidder H, Neufeld G, Klagsbrun M (1996) Characterization of novel vascular endothelial growth factor (VEGF) receptors on tumor cells that bind VEGF165 via its exon 7-encoded domain. *J Biol Chem* **27**: 5761–5767.

Soker S, Takashima S, Miao HQ, Neufeld G, Klagsbrun M (1998) Neuropilin-1 is expressed by endothelial and tumor cells as an isoform-specific receptor for vascular endothelial growth factor. *Cell* **92**: 735–745.

Sugahara KN, Teesalu T, Karmali PP, Kotamraju VR, Agemy L, Girard OM, Hanahan D, Mattrey RF, Ruoslahti E (2009) Tissue-penetrating delivery of compounds and nanoparticles into tumors. *Cancer Cell* **16**: 510–520.

Sugahara KN, Teesalu T, Karmali PP, Kotamraju VR, Agemy L, Greenwald DR, Ruoslahti E (2010) Coadministration of a tumor-penetrating peptide enhances the efficacy of cancer drugs. *Science* **328**: 1031–1035.

Teesalu T, Sugahara KN, Kotamraju VR, Ruoslahti E (2009) C-end rule peptides mediate neuropilin-1-dependent cell, vascular, and tissue penetration. *Proc Natl Acad Sci USA* **106**: 16157–16162.

Tempero M, Plunkett W, Ruiz Van Haperen V, Hainsworth J, Hochster H, Lenzi R, Abbruzzese J (2003) Randomized phase II comparison of dose-intense gemcitabine: thirty-minute infusion and fixed dose rate infusion in patients with pancreatic adenocarcinoma. *J Clin Oncol* **21**: 3402–3408.

Wey JS, Gray MJ, Fan F, Belcheva A, McCarty MF, Stoeltzing O, Somcio R, Liu W, Evans DB, Klagsbrun M, Gallick GE, Ellis LM (2005) Overexpression of neuropilin-1 promotes constitutive MAPK signalling and chemoresistance in pancreatic cancer cells. *Br J Cancer* **93**: 233–241.

Supplementary Information accompanies this paper on British Journal of Cancer website (http://www.nature.com/bjc)

OPEN ACCESS Freely available online

PLOS ONE

Human Subperitoneal Fibroblast and Cancer Cell Interaction Creates Microenvironment That Enhances Tumor Progression and Metastasis

Motohiro Kojima[1☯], Youichi Higuchi[1☯], Mitsuru Yokota[2], Genichiro Ishii[1], Norio Saito[2], Kazuhiko Aoyagi[3], Hiroki Sasaki[3], Atsushi Ochiai[1]*

1 Pathology Division, Research Center for Innovative Oncology, National Cancer Center Hospital East, Kashiwa, Chiba, Japan, **2** Colorectal and Pelvic Surgery Division, National Cancer Center Hospital East, Kashiwa, Chiba, Japan, **3** Genetic Division, National Cancer Center Research Institute, Chuo-ku, Tokyo, Japan

Abstract

Backgrounds: Peritoneal invasion in colon cancer is an important prognostic factor. Peritoneal invasion can be objectively identified as periotoneal elastic laminal invasion (ELI) by using elastica stain, and the cancer microenvironment formed by the peritoneal invasion (CMPI) can also be observed. Cases with ELI more frequently show distant metastasis and recurrence. Therefore, CMPI may represent a particular milieu that facilitates tumor progression. Pathological and biological investigations into CMPI may shed light on this possibly distinctive cancer microenvironment.

Methods: We analyzed area-specific tissue microarrays to determine the pathological features of CMPI, and propagated subperitoneal fibroblasts (SPFs) and submucosal fibroblasts (SMFs) from human colonic tissue. Biological characteristics and results of gene expression profile analyses were compared to better understand the peritoneal invasion of colon cancer and how this may form a special microenvironment through the interaction with SPFs. Mouse xenograft tumors, derived by co-injection of cancer cells with either SPFs or SMFs, were established to evaluate their active role on tumor progression and metastasis.

Results: We found that fibrosis with alpha smooth muscle actin (α-SMA) expression was a significant pathological feature of CMPI. The differences in proliferation and gene expression profile analyses suggested SPFs and SMFs were distinct populations, and that SPFs were characterized by a higher expressions of extracellular matrix (ECM)-associated genes. Furthermore, compared with SMFs, SPFs showed more variable alteration in gene expressions after cancer-cell-conditioned medium stimulation. Gene ontology analysis revealed that SPFs-specific upregulated genes were enriched by actin-binding or contractile-associated genes including α-SMA encoding ACTA2. Mouse xenograft tumors derived by co-injection of cancer cells with SPFs showed enhancement of tumor growth, metastasis, and capacity for tumor formation compared to those derived from co-injection with cancer cells and SMFs.

Conclusions: CMPI is a special microenvironment, and interaction of SPFs and cancer cells within CMPI promote tumor growth and metastasis.

Citation: Kojima M, Higuchi Y, Yokota M, Ishii G, Saito N, et al. (2014) Human Subperitoneal Fibroblast and Cancer Cell Interaction Creates Microenvironment That Enhances Tumor Progression and Metastasis. PLoS ONE 9(2): e88018. doi:10.1371/journal.pone.0088018

Editor: Soroku Yagihashi, Hirosaki University Graduate School of Medicine, Japan

Received September 27, 2013; **Accepted** January 2, 2014; **Published** February 4, 2014

Funding: This work was supported by JSPS KAKENHI grant number 24590458, and a grant of a 3rd-term Comprehensive 10-year Strategy for Cancer Control (23-A-3). The funders had no role in study design, data collection and analysis, decision to publish, or preparation of the manuscript.

Competing Interests: The authors have declared that no competing interests exist.

* E-mail: aochiai@east.ncc.go.jp

☯ These authors contributed equally to this work.

Introduction

Although tumor size is a major prognostic factor in many cancers, prognosis in gastrointestinal cancer is stratified not by tumor size but by tumor spread [1]. Peritoneal invasion in colorectal cancer has been reported to be a strong prognostic factor, but this term was not well defined, and detection and diagnosis methods have been questioned [2–4]. Recent pathological reports have demonstrated that elastica stain, which highlights the peritoneal elastic lamina near the periotoneal surface, is useful for objective detection of peritoneal invasion. We and others have determined that peritoneal invasion defined as tumor invasion beyond the peritoneal elastic lamina (elastic laminal invasion: ELI) is a strong prognostic factor that can influence future pT criteria in the Union for International Cancer Control (UICC) TNM classification [5–7]. The peritoneum is a very thin membrane, within 500 μm thick, and the peritoneal elastic lamina exists within this membrane. The frequency of synchronous metastasis and recurrence is increased by 2 to 4 times when a tumor invades this narrow space [5]. These results may suggest that tumor progression and metastasis are facilitated by a cancer microenvironment formed by peritoneal invasion (CMPI). The extent of

CMPI can be identified by using elastica stain, and pathological features of CMPI can also be determined.

A tissue microarray facilitates the evaluation of protein expression for a large number of tissue blocks from a single specimen, and area-specific tissue microarrays have been reported to be useful for studying specific tumor areas in large cohorts [8]. After determination of CMPI by using elastica stain, a tissue core can be obtained from this area and a comparison with the features of other tumor areas can also be performed. This process may allow for an assessment of the important biological phenomena occurring in this cancer microenvironment.

Recent advances in cancer research have established the concept of cancer microenvironment that promotes tumor initiation, invasion, and metastasis [9]. Although the cancer microenvironment is composed of many types of cells, the use of area-specific tissue microarrays may allow for a focus on the cell components that characterize CMPI. Furthermore, if these cell components can be cultivated from the histologically corresponding subperitoneal region, a biological study to elucidate this putative cancer-promoting microenvironment can be performed.

The aim of this study was to explain how the colorectal cancer prognosis is affected by peritoneal invasion. We constructed area-specific tissue microarray system to determine the characteristic cell components of CMPI. Next, we cultivated specific fibroblast subpopulations from the submucosal and subperitoneal layers of the human colonic wall. The biological characteristics and gene profiles of submucosal fibroblasts (SMFs) and subperitoneal fibroblasts (SPFs) with or without cancer-cell-conditioned medium (CCCM) stimulation were compared. Subsequently, we constructed xenograft tumors by co-injection of cancer cells with either SPFs or SMFs. Our study proposed a new candidate for a cancer-promoting microenvironment in colon cancer and elucidated SPFs as crucial players in the enhancement of tumor progression and metastasis.

Patients and Methods

Ethics Statement

This study was approved by the National Cancer Center Hospital East Institutional Review Board (No: 19-021). A written general consent to use biologic materials for research was obtained from each participant prior to tissue acquisition. Animal experiments were approved by the Animal Ethics Committee of the National Cancer Center Hospital East (K11-032).

Patient Characteristics and Detection of ELI

Four hundred consecutive patients with TNM classification (5^{th} edition) pT3 and pT4a colon cancer [10], undergoing surgery between 1996 and 2003 at the National Cancer Center Hospital East, were enrolled. Using elastica stain, we identified 173 cases with ELI and further examined these using area-specific tissue microarrays [5,8]. Of the 173 cases with ELI, 107 were pT3 and 66 were pT4a.

Construction of Area-Specific Tissue Microarrays

To elucidate the pathological features of CMPI in colon cancer tissue, we defined the cancer microenvironment as follows: (a) CMPI has a tumor border with peritoneal invasion and (b) the cancer microenvironment formed by submucosal invasion (CMSI) has a submucosal invasive tumor border (Figure 1A) [5]. The 2-point tissue microarray was then established as previously described [8]. Each tumor area was marked with ink on the histological slide; a single tissue core of 2 mm in diameter was obtained from each cancer microenvironment and transferred to a recipient block using a Tissue Microarrayer (Azumaya, Tokyo, Japan). In 24 cases, insufficient cancer tissue was obtained from the CMPI. However, sufficient tissue was obtained in 149 cases; these were analyzed histologically and immunohistochemically (See Materials and Methods S1, and Table S1).

Antibodies, Regents, and Immunohistochemistry

The antibodies, reagents, and the immunohistochemical procedures used are described in Materials and Methods S1 and the Table S2.

Evaluation of Area-Specific Tissue Microarray Sections

High-resolution slide images were acquired from all tissue cores with hematoxylin-eosin (H.E) and immunohistochemistry staining, using NanoZoomer 2.0-HT slide scanner (Hamamatsu photonics, Hamamatsu, Japan). All cores were examined using viewer software (NDP view: Hamamatsu photonics, Hamamatsu, Japan). When the area of fibrosis exceeded 50% of a whole tissue core with a 2 mm diameter upon H.E staining, it was defined as positive for marked fibrosis. On immunohistochemical staining, hot spots with CD3-, CD31-, and CD68-positive cells or vessels were selected in the viewer software, then an image of x20 magnification (0.51 mm^2) was taken, and saved as a JPEG file. Positive cells or vessels were counted in each image using morphometric software (WinRoof, Mitani Corporation, Fukui, Japan). Moreover, the area with highest alpha smooth muscle actin (α-SMA) expression in fibroblasts was selected, then a x20 magnification (0.51 mm^2) image was taken, and saved as a JPEG file. The ratio of the α-SMA positive area in the image was calculated using morphometric software, as described previously [11]. The α-SMA expression in normal muscle tissue, as determined by comparison with a serial H.E slide, was not evaluated. H.E and immunohistochemical staining data of CMPI was compared with that of CMSI to elucidate the histological characteristics of CMPI.

Primary Cells and Cell Lines

Submucosal tissue was obtained from sigmoid colon tissue more than 5 cm distant from the tumor. Colonic tissue was dissected from the muscular layer on the luminal side, and lamina propria and mucosal layer tissues were obtained. Next, the lamina propria was scrubbed away to obtain submucosal tissue. Subperitoneal tissue was obtained from the sigmoid colon mesentery at more than 5 cm distant from the tumor by using operating tweezers and scissors. These tissues were washed with phosphate-buffered saline (PBS) and incubated in 5% trypsin for 20 minutes, 3 times. The supernatant was centrifuged, plated on a dish, and submucosal fibroblasts (SMFs) and subperitoneal fibroblasts (SPFs) were obtained and then grown and maintained in MF-medium (Toyobo, Tokyo, Japan) [12]. All experiments were performed on cells within 8 passages.

The human colorectal cancer cell lines DLD-1 and Caco-2 were obtained from the American Type Culture Collection and grown in Dulbecco's modified Eagle medium (DMEM) (Sigma-Aldrich, Saint Louis, MO) containing 100 U/mL penicillin, 100 μg/mL streptomycin (Sigma-Aldrich, Saint Louis, MO), and 10% fetal bovine serum (FBS; Gibco, Palo Alto, CA).

Cell Proliferation Assay, Immunocytochemical Staining, and Flow Cytometry Analysis

Cell proliferation assays, immunocytochemical staining, and flow cytometry analyses were performed as described in Materials and Methods S1.

Stimulation of Fibroblasts by Cancer Cell Medium

Initially, $1.7\times10^4/cm^2$ of fibroblasts and DLD-1 cells were grown separately in DMEM containing 100 U/mL penicillin, 100 μg/mL streptomycin, and 10% FBS for 48 hours, and then were starved for 24 hours. Next, the medium was removed from the fibroblasts, and the medium from the starved DLD-1 cells was added to the fibroblasts for 24 hours to establish fibroblasts with cancer-cell-conditioned medium (CCCM) stimulation. As control, fibroblasts were starved for 48 hours (yielding fibroblasts without CCCM). SPFs and SMFs either with or without CCCM were assessed by using immunocytochemistry or gene expression analysis. As for the evaluation of immunocytochemical α-SMA expression, the area with highest α-SMA expression was selected, then a x20 magnification (0.51 mm^2) image was taken, and saved as a JPEG file. The ratio of α-SMA positive area in the image was calculated using morphometric software (WinRoof, Mitani Corporation, Fukui, Japan).

Gene Expression Analysis using Microarray

Three sets of SPFs and SMFs, either with or without CCCM, obtained from 3 different patients, were used in this study. We used GeneChip Human Genome U133 Plus 2.0 arrays (Affymetrix, Santa Clara, CA). Target cDNA was generated from 100 ng of total RNA extracted from each sample using a 3′ IVT Express Kit (Affymetrix, Santa Clara, CA). The procedures for target hybridization, washing and staining for signal amplification were performed according to the supplier's protocols. The arrays were scanned with a Gene Chip Scanner 3000 (Affymetrix, Santa Clara, CA), and the intensity of each feature of the array was calculated by using GeneChip Operating Software, version 1.1.1 (Affymetrix, Santa Clara, CA). The average intensity was standardized to the target intensity, which was set equal to 1000, to reliably compare different arrays. The values were log transformed and median centered. The programs GeneSpring (Agilent Technologies, Santa Clara, CA) and Excel (Microsoft Corporation, Redmond, WA) were used to perform the numerical analyses for gene selection.

Xenograft Transplantation and Tumor Formation Assay

Either 1×10^6 human colorectal cancer cells Caco-2 or DLD-1 alone, or with either 1×10^6 SPFs or SMFs, were injected subcutaneously (s.c.) into the back of SCID mice (8–12 weeks of age; CLEA, Tokyo, Japan). Tumor volumes were calculated weekly as described previously [13]. Mice injected with Caco-2 alone or with either SPFs or SMFs were killed after 10 weeks, and those injected with DLD-1 alone or with either SPFs or SMFs were killed after 8 weeks, and tumor weights were evaluated. For distant metastatic analysis, lung and liver tissue was removed and fixed in 10% formalin, and for the analysis of lymph node metastasis, neck and inguinal adipose tissue was also removed and fixed; all tissues were histologically examined. We used 8 mice in each group.

To elucidate the capacity of fibroblasts to enhance tumor formation, serial dilutions of Caco-2 or DLD-1 cancer cells were similarly co-injected with either 1×10^6 SMFs or SPFs. Tumor formation was evaluated 4 weeks after the injection. We used 4 mice for each group.

Statistical Analysis

X^2 test and Student's t test were used in the tissue microarray analysis, cell proliferation assay, xenograft transplantation, and tumor formation assay. A $P<0.05$ was defined as statistically significant. In the microarray analysis, gene expression data were analyzed using GeneSpring GX12 (Agilent Technologies, Santa Clara, CA). Row data were summarized by using MAS5 and normalized by log transformation and median centering for numerical analyses for gene selection. For principal component analysis (PCA), we used probe sets that were reliably measured and varied by 3-fold above the global median in at least 2 samples (approximately 10%); analyses were performed using GeneSpring GX12. The differentially expressed probe sets used in supervised hierarchical clustering were selected based on $P<0.05$ and fold change (FC) >2.0. P values were calculated using one way ANOVA with Benjamini and Hochberg FDR multiple testing correction. Hierarchical clustering with weight-average linkage clustering was performed using Cluster and Treeview programs (Michael Eisen, Stanford University, genome-www.stanford.edu). The functional annotation clustering of Gene Ontology Enrichment analysis was performed using DAVID software, with the classification stringency set to "High", and the significant clusters were selected based on an enrichment score >2.0 and a $P<0.01$ (Fisher's exact test after Benjamini and Hochberg FDR multiple testing correction) [14,15].

Results

Histological Features of ELI

Not only tumor cells, but also varieties of stromal cells constitute a distinct cancer microenvironment, and some promote tumor metastasis [9]. First, we elucidated the significant histological features of CMPI to shed light on phenomena occurring in this milieu by using area-specific tissue microarrays. The clinicopathological features of the 149 cases used are shown in Table S1. On H.E staining, we found extensive fibrosis (over 50%) more frequently in CMPI than was seen in CMSI (Figure 1B). The ratio of α-SMA positive area in CMPI was also higher than that seen in CMSI (Figure 1C). The proportions of T lymphocytes, macrophages, or microvessels evaluated using CD3, CD68, or CD31, respectively, were not significantly different between CMPI and CMSI (Figure 1D–F). Both in CMPI and CMSI, plump spindle-shaped fibroblasts were major source of α-SMA expression, and the ratio was successfully analyzed by using morphometric software (Figure 2A–D). Considering our previous results, which indicated that peritoneal invasion defined by ELI was closely associated with distant metastasis, we hypothesized that fibroblasts in the subperitoneal layer could be implicated not only in prominent fibrosis and activation, but also in the tumor's progression and metastasis. We then decided to isolate fibroblasts from the subperitoneal layer that histologically corresponded to peritoneal invasion. Fibroblasts from the submucosal layer were used as controls.

Isolation and Characterization of Cultured Human SPFs and SMFs

At first, we evaluated the morphological and biological characteristics of SPFs and SMFs in a normal state. Both cultured human SPFs and SMFs showed similar spindle-shaped morphologic characteristics (Figure S1A–B). SPFs and SMFs from 3 patients could be cultured over 10 passages, except for 1 SPF case (data not shown). Immunocytochemistry and flow cytometry revealed the obtained SPFs and SMFs were consistent with fibroblasts (Figure S1C–D). We found weak α-SMA expression in a few SPFs and SMFs. The doubling time for SPFs and SMFs was 79.9 hours and 36.3 hours, respectively, and the growth of SMFs was faster than that of SPFs ($P<0.05$), which suggested a biological difference between SPFs and SMFs (Figure S1E).

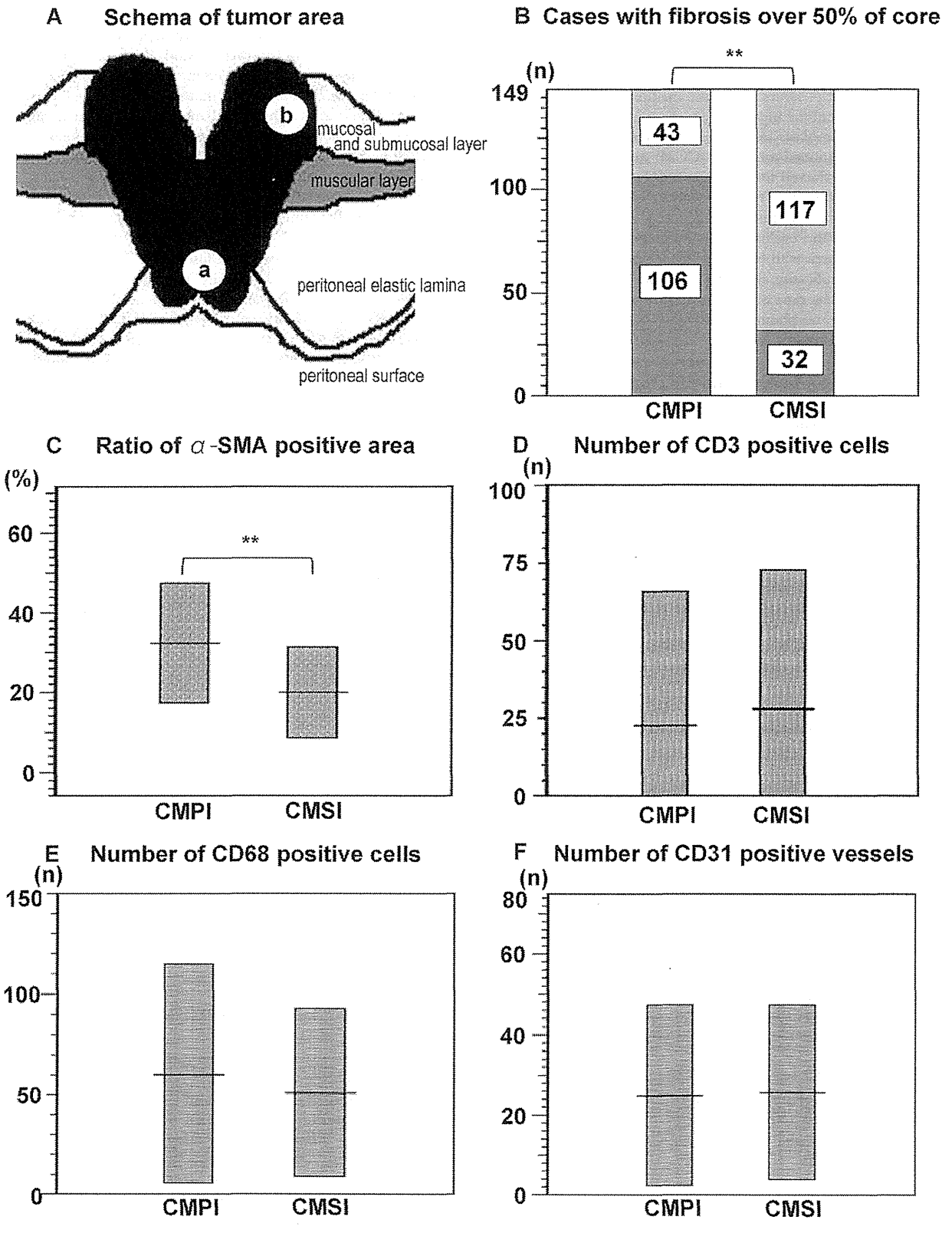

Figure 1. Pathological features of tumor microenvironment explored by using area-specific tissue microarray. (A) Schema of the cancer microenvironment formed by peritoneal invasion (CMPI) and the cancer microenvironment formed by submucosal invasion (CMSI) defined as

(a) invasive front with peritoneal invasion and (b) submucosal invasive front, respectively. (B) The distribution of fibrosis in human colon cancer tissue. Dark gray bars show the number of the cases with fibrosis over 50% of the core from each tumor area, and light gray bars show the number of the cases without extensive fibrosis. Core samples with CMPI showed a higher frequency of marked fibrosis than did core samples with CMSI ($P<0.01$). (C) Distribution of α-SMA expression in human colon cancer tissue. CMPI showed higher α-SMA expressions than those seen in CMSI ($P<0.01$). (D) Distribution of CD3-positive cells in human colon cancer tissue. Numbers of CD3-positive cells were not significantly different between CMPI and CMSI. (E) Distribution of CD68-positive cells in human colon cancer tissue. Numbers of CD68-positive cells were not significantly different between CMPI and CMSI. (F) Distribution of CD31-positive vessels in human colon cancer tissue. Numbers of the CD31-positive vessels were not significantly different between CMPI and CMSI. Results in (B) are presented by case numbers, and those in (C–F) are presented as the mean ± SD of 149 cases (**$P<0.01$).

doi:10.1371/journal.pone.0088018.g001

Gene Expression Profiling Comparison between SPFs and SMFs

To assess the phenotypical differences between SPFs and SMFs, the gene expression profiles of fibroblasts with or without CCCM stimulation were compared. PCA revealed 4 distinct clusters, depending on their origin and CCCM stimulation, which overcame the individual variation (Figure 3A and B). Supervised cluster analysis also revealed 4 distinct clusters (Figure 3C). This indicated the phenotypical difference in fibroblasts within the colonic wall. And this difference depended on the histoanatomical location. Furthermore, the reaction to CCCM stimulation was also different.

Next, we compared gene expression profiles in these fibroblasts with and without CCCM stimulation, separately (Figure 3D–E). Data from SPFs without CCCM stimulation were enriched by the gene ontology (GO) terms "extracellular matrix" and "proteinaceous extracellular matrix", which formed annotation cluster 1. Major expracellular matrix (ECM) components of collagens (COL1A1, COL4A1, COL4A2, COL5A1, and COL16A1), laminin, or fibronectin were included in this cluster. Moreover, gene expression related to components that bind to the ECM was also upregulated in SPFs and formed annotation cluster 2. Annotation cluster 3 was enriched for GO terms associated with "granules" or "vesicles" (Figure 3D and Table S3). This result suggested the gene expression profile associated with basic function in fibroblasts is different between SPFs and SMFs within the colonic wall. The top 20 genes highly expressed in SPFs also included several ECM components. Genes associated with fibrogenesis or the myofibroblastic differentiation of FLI1 and NOX4 were also found in the top 20 genes (Table S4). Among other highly expressed genes in SPFs without CCCM stimulation, we found POSN, SPARC, or COL4A1, which are known to be highly expressed in the cancer stroma; and many of these are prognostic factors [11,16,17].

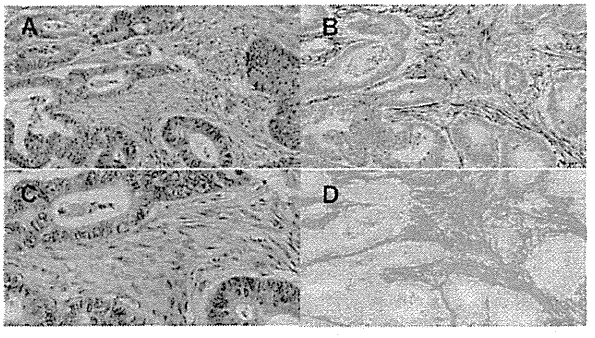

Figure 2. Histological features of fibrosis in the cancer microenvironment formed by peritoneal invasion (CMPI). (A) Histological features of stromal component of CMPI. Both in CMPI and the cancer microenvironment formed by submucosal invasion (CMSI), plump spindle-shaped fibroblasts were major sources of the stroma. (B) Marked α-SMA expression was found in fibroblasts. (C) Higher magnification more clearly revealed plump spindle-shaped fibroblasts. (D) Using morphometric software, we successfully detected and analyzed α-SMA expression.

doi:10.1371/journal.pone.0088018.g002

Most of the genes with increased expressions in SPFs without CCCM stimulation were also retained in the presence of CCCM stimulation; however, there were some differences (Figure 3D–E, Table S5–6). In GO analysis of SPFs with CCCM stimulation, the order of annotation clusters were changed compared to that seen in SPFs without CCCM stimulation. Among the top 20 genes, 13 genes were conserved and 7 genes were replaced. These results suggest a difference in the reaction to CCCM stimulation between SPFs and SMFs. The existence of SPFs-specific genes that are upregulated after CCCM stimulation was estimated.

We then analyzed these genes to establish the biological characteristics of SPFs after exposure to CCCM. A Venn diagram revealed 193 upregulated genes in SPFs and 59 in SMFs after CCCM stimulation. Of these, 51 were commonly upregulated both in SPFs and SMFs, 142 were SPFs specific, and only 8 were SMFs specific (Figure 4A). We then also focused on downregulated genes, and discovered 215 in SPFs and 146 in SMFs. Of these, 138 were commonly downregulated both in SPFs and SMFs, 77 were SPFs specific, and only 8 were SMFs specific (Figure 4B). These results suggested that SPFs showed more variable alteration in gene expression after CCCM stimulation. GO term analysis of SPF-specific genes downregulated after CCCM stimulation did not revealed any annotation cluster over 3.0 of the enrichment score (data not shown). In contrast, GO term analysis of SPFs-specific genes upregulated after CCCM stimulation revealed that terms such as "actin binding", "cytoskeletal binding protein", "contractile fiber", "LIM domain", "contractile fiber part", "sarcomere", and "myofibril" formed annotation cluster 1–3 (Figure 4C). Most of these genes were known to be related to cell contraction. Among the top 20 genes were many cytoskeletal or contractility associated genes. Surprisingly, ACTA2 that encodes α-SMA was upregulated specifically in SPFs after CCCM stimulation (Figure 4D). This result was confirmed by immunocytochemistry (Figure 4E–F). Morphometric analysis in immunocytochemical expression revealed that α-SMA expression was upregulated specifically and significantly in SPFs after CCCM stimulation in protein level (Figure S2, $P<0.05$). Variable upregulation and downregulation of genes after CCCM stimulation was a significant feature in SPFs. ACTA2 encoding α-SMA was included in this SPFs-specific upregulated gene set. Cancer associated fibroblasts (CAFs) include α-SMA-positive activated myofibroblasts. Together with the result of area-specific tissue microarrays, marked α-SMA expression in CMPI is depended on the sensitive character of SPFs which may associated with the difference in cancer microenvironment.

SPFs Enhance Tumor Growth, Metastasis and Tumor Formation Ability more Strongly than do SMFs

To elucidate the functional differences of fibroblasts in the colonic wall, we injected human colorectal cancer cell lines Caco-2

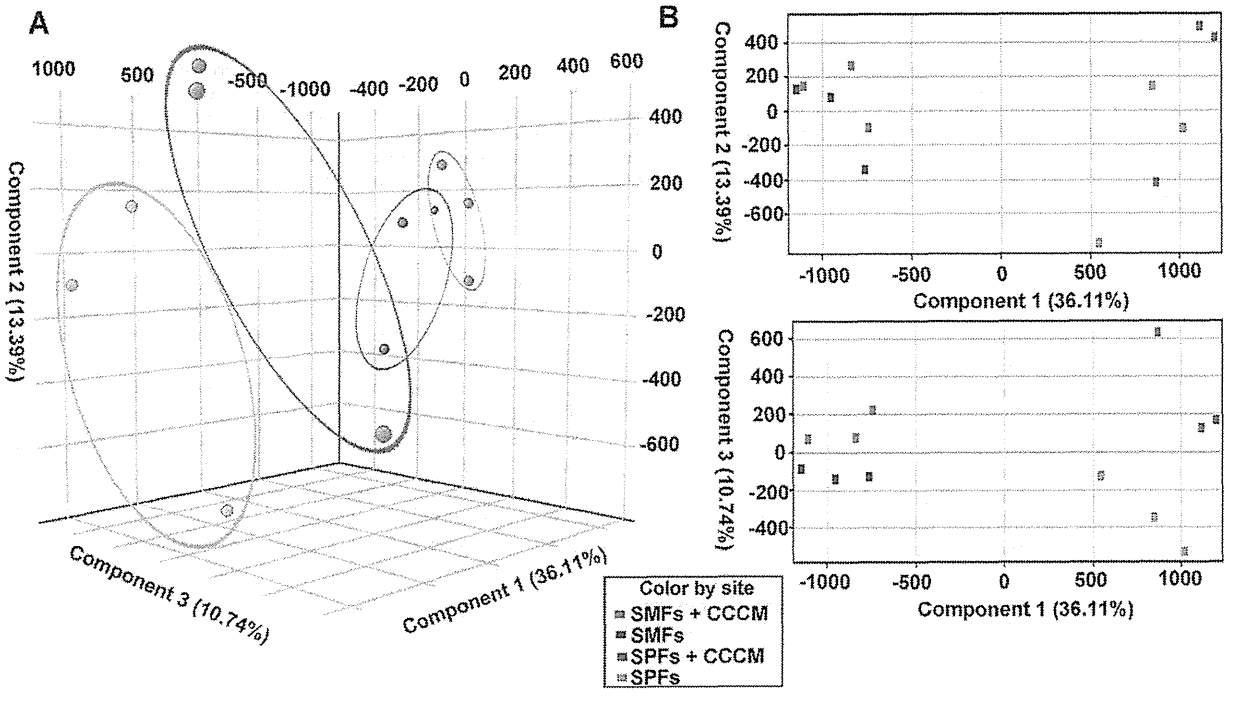

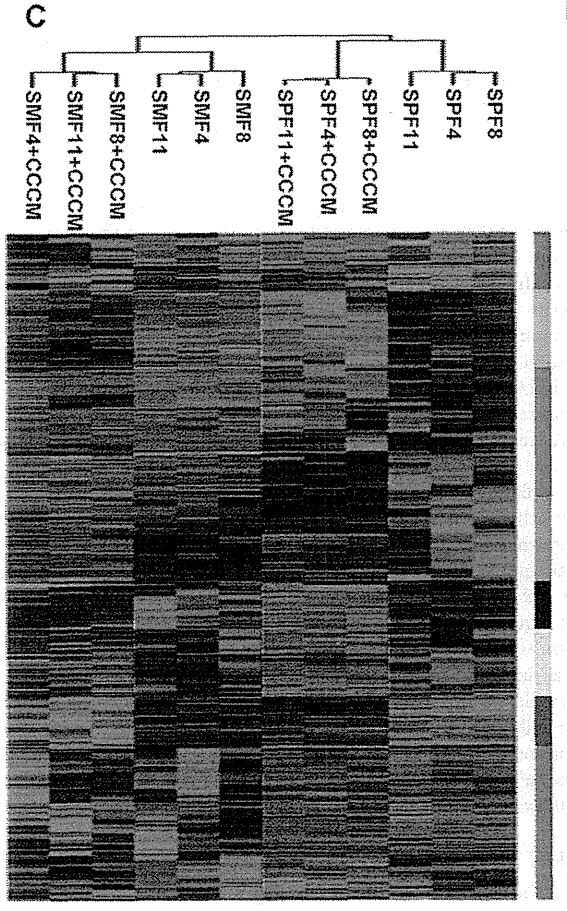

D

Upregulated gene clusters in SPFs compared with SMFs

Annotation Cluster 1	Enrichment Score: 9.31	
Gene Ontology ID	Gene Ontology Term	*P* value
GO:0031012	extracellular matrix	< .01
GO:0005578	proteinaceous extracellular matrix	< .01
SP_PIR_KEYWORDS	extracellular matrix	< .01
Annotation Cluster 2	Enrichment Score: 3.92	
Gene Ontology ID	Gene Ontology Term	*P* value
GO:0030247	polysaccharide binding	< .01
GO:0001871	pattern binding	< .01
GO:0005539	glycosaminoglycan binding	0.02
GO:0030246	carbohydrate binding	0.05
Annotation Cluster 3	Enrichment Score: 3.92	
Gene Ontology ID	Gene Ontology Term	*P* value
GO:0031093	platelet alpha granule lumen	< .01
GO:0060205	cytoplasmic membrane-bounded vesicle lumen	< .01
GO:0031983	vesicle lumen	< .01
GO:0031091	platelet alpha granule	< .01
GO:0030141	secretory granule	0.09
GO:0044433	cytoplasmic vesicle part	0.29

E

Upregulated gene clusters in SPFs with CCCM stimulation compared with SMFs with CCCM stimulation

Annotation Cluster 1	Enrichment Score: 10.12	
Gene Ontology ID	Gene Ontology Term	*P* value
SP_PIR_KEYWORDS	extracellular matrix	<.01
GO:0031012	extracellular matrix	<.01
GO:0005578	proteinaceous extracellular matrix	<.01
Annotation Cluster 2	Enrichment Score: 4.92	
Gene Ontology ID	Gene Ontology Term	*P* value
GO:0016477	cell migration	<.01
GO:0048870	cell motility	<.01
GO:0051674	localization of cell	<.01
Annotation Cluster 3	Enrichment Score: 4.66	
Gene Ontology ID	Gene Ontology Term	*P* value
GO:0001871	pattern binding	<.01
GO:0030247	polysaccharide binding	<.01
GO:0005539	glycosaminoglycan binding	<.01
GO:0030246	carbohydrate binding	0.11

Figure 3. Gene expression profiles in subperitoneal fibroblasts (SPFs) and submucosal fibroblasts (SMFs) with and without cancer-cell-conditioned medium (CCCM) stimulation. (A) Red is the microarray profile in SMFs with CCCM stimulation, blue is SMFs without CCCM stimulation, green is SPFs with CCCM stimulation, and silver is SPFs without CCCM stimulation. Three-dimensional representation of principal component analysis (PCA) component 1, 2, and 3. (B) Two dimensional representation of PCA components 1 and 2 (upper), and PCA components 1 and 3 (lower). Fibroblasts formed independent clusters, depending on histoanatomical site and the presence of CCCM stimulation. (C) Supervised cluster analysis in fibroblasts also revealed distinct clusters depending on histoanatomical site and the presence of CCCM stimulation. (D) Gene ontology analysis of upregulated genes in SPFs compared with SMFs. (E) Gene ontology analysis of genes upregulated in SPFs with CCCM stimulation, compared with SMFs with CCCM stimulation. Most of the genes with increased expressions in SPFs were retained after CCCM stimulation; however, there were some differences, and the order of annotation clusters were changed after CCCM stimulation.
doi:10.1371/journal.pone.0088018.g003

or DLD-1 s.c., alone, or along with either SPFs or SMFs, into SCID mice. At 7 weeks after the injection, all mice demonstrated tumor formation. The growth of tumors arising from cancer cells injected along with SPFs grew faster than that arising from the injection of cancer cells alone or co-injection with SMFs (Figure 5A). The final weights of tumors arising from cancer cells co-injected with SPFs were also larger than those arising from the injection of cancer cells alone or from co-injection with SMFs

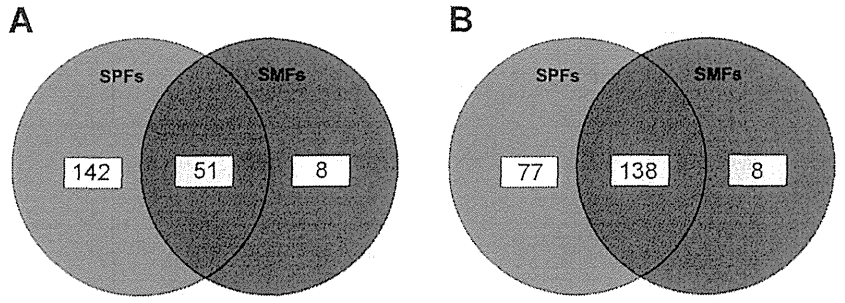

C SPFs specific upregulated gene cluster after CCCM stimulation

Annotation Cluster 1	Enrichment Score: 4.73	
Gene Ontology ID	Gene Ontology Term	*P* value
GO:0003779	actin binding	< .01
SP_PIR_KEYWORDS	actin-binding	< .01
GO:0008092	cytoskeletal protein binding	0.01
Annotation Cluster 2	Enrichment Score: 3.97	
Gene Ontology ID	Gene Ontology Term	*P* value
SP_PIR_KEYWORDS	LIM domain	< .01
INTERPRO	IPR001781:Zinc finger, LIM-type	< .01
SMART	SM00132:LIM	< .01
Annotation Cluster 3	Enrichment Score: 3.84	
Gene Ontology ID	Gene Ontology Term	*P* value
GO:0044449	contractile fiber part	< .01
GO:0043292	contractile fiber	< .01
GO:0030017	sarcomere	< .01
GO:0030016	myofibril	< .01

D Top 20 in SPFs specifically upregulated genes after CCCM stimulation

Probe Set ID	*P* value	FC	Gene Symbol
206029_at	< .01	13.41	ANKRD1
206825_at	< .01	10.84	OXTR
205795_at	< .01	8.67	NRXN3
210511_s_at	< .01	8.09	INHBA
204671_s_at	< .01	7.66	ANKRD6
212473_s_at	< .01	7.57	MICAL2
202628_s_at	< .01	6.96	SERPINE1
229669_at	< .01	6.75	LOC100507263
201195_s_at	< .01	6.61	SLC7A5
200974_at	< .01	6.52	ACTA2
205518_s_at	< .01	6.49	CMAH
217452_s_at	< .01	6.32	B3GALT2
205442_at	< .01	6.21	MFAP3L
1558828_s_at	< .01	6.2	LOC728264
223063_at	< .01	5.84	C1orf198
204589_at	< .01	5.59	NUAK1
226869_at	< .01	5.44	MEGF6
213067_at	< .01	5.43	MYH10
203432_at	< .01	5.14	TMPO
206117_at	< .01	5.09	TPM1

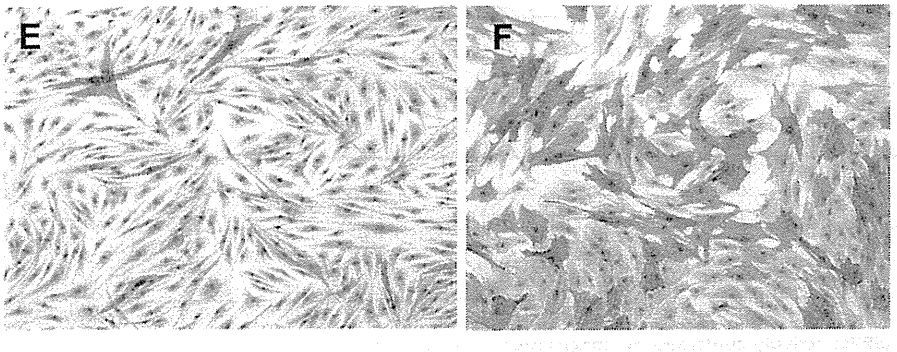

Figure 4. Gene modification in subperitoneal fibroblasts (SPFs) after cancer-cell-conditioned medium (CCCM) stimulation. (A) Genes upregulated by CCCM stimulation. (B) Genes downregulated by CCCM stimulation. (C) Top 3 annotation clusters in gene ontology analysis of SPFs-specific genes upregulated by CCCM stimulation. (D) Top 20 genes upregulated specifically in SPFs after CCCM stimulation. (E) Immunocytochemical α-SMA expression in SMFs after CCCM stimulation. (F) Immunocytochemical α-SMA expression in SPFs after CCCM stimulation. α-SMA expression was upregulated specifically in SPFs after CCCM stimulation (see also Figure S2).
doi:10.1371/journal.pone.0088018.g004

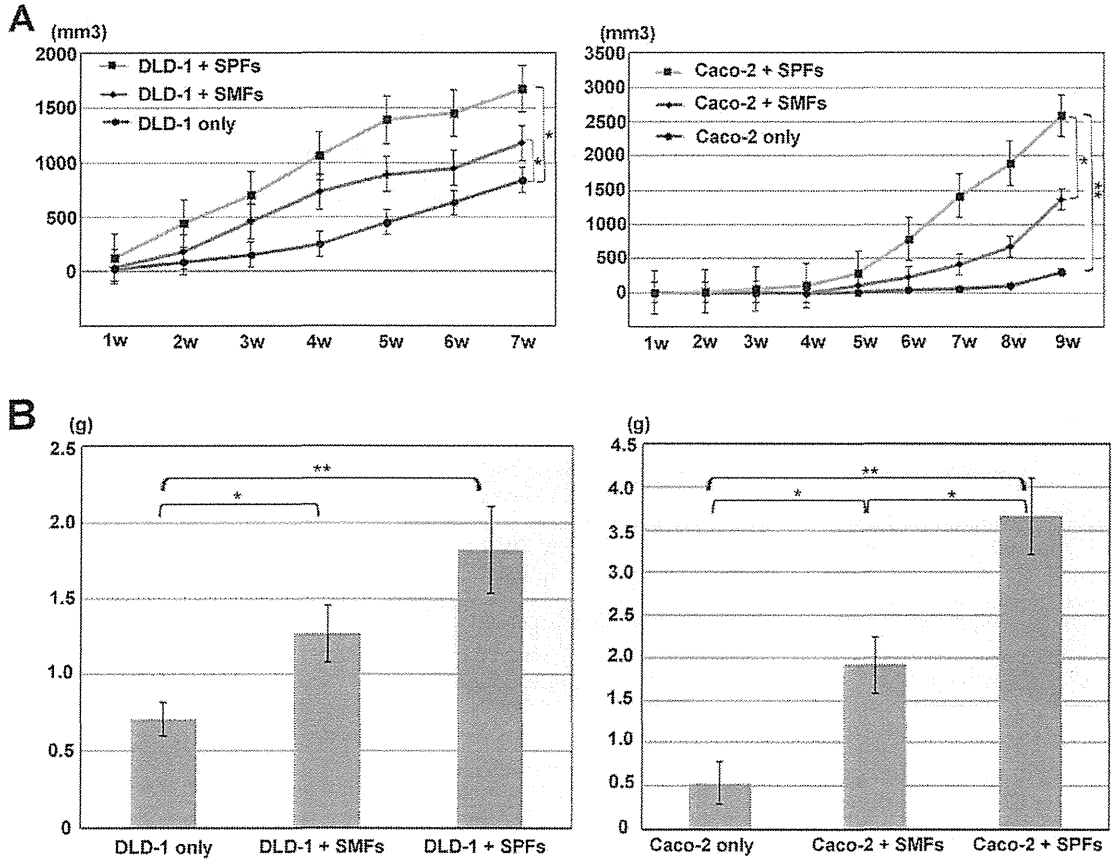

C

	Liver metastasis	Lung metastasis	Lymph node
Caco-2 + SPFs (10 weeks)	0/8	0/8	0/8
Caco-2 + SMFs (10 weeks)	0/8	0/8	0/8
DLD-1 + SPFs (8 weeks)	0/8	0/8	**4/8**
DLD-1 + SMFs (8 weeks)	0/8	0/8	**2/8**

D

Cells inoculated	Number of cancer cells	Tumor formation rate
Caco-2 only	1×10^6	0/4
Caco-2 + SPFs (1×10^6)	1×10^6	4/4
Caco-2 + SMFs (1×10^6)	1×10^6	4/4
Caco-2 only	5×10^5	0/4
Caco-2 + SPFs (1×10^6)	5×10^5	4/4
Caco-2 + SMFs (1×10^6)	5×10^5	4/4
Caco-2 only	1×10^5	0/4
Caco-2 + SPFs (1×10^6)	1×10^5	4/4
Caco-2 + SMFs (1×10^6)	1×10^5	3/4
Caco-2 only	5×10^4	0/4
Caco-2 + SPFs (1×10^6)	5×10^4	2/4
Caco-2 + SMFs (1×10^6)	5×10^4	0/4

Cells inoculated	Number of cancer cells	Tumor formation rate
DLD-1 only	1×10^6	3/4
DLD-1 + SPFs (1×10^6)	1×10^6	4/4
DLD-1 + SMFs (1×10^6)	1×10^6	4/4
DLD-1 only	5×10^5	1/4
DLD-1 + SPFs (1×10^6)	5×10^5	4/4
DLD-1 + SMFs (1×10^6)	5×10^5	4/4
DLD-1 only	1×10^5	0/4
DLD-1 + SPFs (1×10^6)	1×10^5	4/4
DLD-1 + SMFs (1×10^6)	1×10^5	1/4
DLD-1 only	5×10^4	0/4
DLD-1 + SPFs (1×10^6)	5×10^4	3/4
DLD-1 + SMFs (1×10^6)	5×10^4	1/4

Figure 5. Subperitoneal fibroblasts (SPFs) actively contribute to cancer progression. (A, left) Xenograft tumor growth in mice injected with DLD-1 human colorectal cancer cells alone (blue line, 840.7±112.6 mm^3 in 7 weeks), co-injected with DLD-1 cells and submucosal fibroblasts (SMFs; red line, 1178.0±177.6 mm^3 in 7 weeks), and co-injected with DLD-1 cells and subperitoneal fibroblasts (SPFs; green line, 1672.8±214.7 mm^3 in 7 weeks). The differences of tumor volume between DLD-1 cells alone and DLD-1 cells with SPFs, and between DLD-1 cells alone and DLD-1 cells with SMFs were statistically significant ($P<0.05$). (A, right) Xenograft tumor growth in mice injected with Caco-2 human colorectal cancer cells alone (blue line, 308.6±127.7 mm^3 in 9 weeks), co-injected with Caco-2 cells and SMFs (red line, 1363.1±284.3 mm^3 in 9 weeks), and co-injected with Caco-2 and SPFs (green line, 2595.1±349.5 mm^3 in 9 weeks). The differences of tumor volume between Caco-2 cells alone and Caco-2 cells with SPFs ($P<$

0.01), and between Caco-2 cells with SMFs and Caco-2 cells with SPFs ($P<0.05$) were statistically significant. Xenograft tumors derived from co-injection of cancer cells and SPFs grew faster than those derived from injection of cancer cells alone, or co-injection of cancer cells and SMFs. (B, left) Xenograft tumor weight in mice injected with DLD-1 cells alone was 0.71±0.11 g, co-injected with DLD-1 cells and SMFs was 1.27±0.19 g, and co-injected with DLD-1 cells and SPFs was 1.82±0.28 g in 8 weeks. The differences of tumor weight between DLD-1 cells alone and DLD-1 cells with SPFs ($P<0.01$), and between DLD-1 cells alone and DLD-1 cells with SMFs ($P<0.05$) were statistically significant. (B, right) Xenograft tumor weight in mice injected with Caco-2 cells alone was 0.53±0.24 g, co-injected with Caco-2 cells and SMFs was 1.91±0.34 g, and co-injected with Caco-2 cells and SPFs was 3.66±0.45 g in 10 weeks. The differences of tumor weight between DLD-1 cells alone and DLD-1 cells with SPFs ($P<0.01$), between DLD-1 cells alone and DLD-1 cells with SMFs ($P<0.05$), and between DLD-1 cells with SPFs and DLD-1 cells with SMFs ($P<0.05$) were statistically significant. Weights of xenograft tumors derived from co-injection of cancer cells with SPFs were higher than those of tumors derived from injection of cancer cells alone, or co-injection of cancer cells and SMFs (left: DLD-1, right: Caco-2). (C) Although the value did not reach statistical significance, xenograft tumors derived from co-injection of DLD-1 cells and SPFs showed twice the frequency of lymph node metastasis (n = 4) compared to those deriving from co-injection of DLD-1 cells and SMFs (n = 2). (D) Co-injection of cancer cells and SPFs result in enhanced tumor formation capacity. Results are presented as the mean ± SE of 8 mice (*$P<0.05$. **$P<0.01$).
doi:10.1371/journal.pone.0088018.g005

(Figure 5B). Although the difference was not statistically significant, tumors arising from the co-injection of DLD-1 cells with SPFs more frequently resulted in lymph node metastasis than did those formed from the co-injection of DLD-1 cells with SMFs (Figure 5C).

Next, the cancer cells being injected were serially diluted and tumor formation was evaluated at 4 weeks after the injection, as described previously [13]. Comparison with mice injected with cancer cells alone or co-injected with cancer cells and SMFs, enhanced tumor formation was found in mice co-injected with cancer cells and SPFs, and tumor formation was observed even when the injected cells were diluted to 5×10^{4} (Caco-2) or 1×10^{4} (DLD-1). These results suggested that SPFs enhanced tumor growth, metastasis, and tumor formation capacity, in comparison with the effect of SMFs; these findings may be related to the peritoneal invasion dependent clinical outcome in colon cancer.

Discussion

Fibroblasts are one of the most common types of stromal cells in connective tissue. Fibroblasts and loose connective tissue, which is one morphological type of connective tissue, are present throughout the body and contribute to the maintenance of the structural framework of most tissues, including the gastrointestinal tract [18]. Histologically, the gastrointestinal tract is composed of 5 layers that consist of the lamina propria, submucosa, muscular layer, subserosa, and serosa. Loose connective tissue and fibroblasts exist in every layer and have distinct physiological and pathological functions [19,20].

SPFs are known to produce peritoneal fluid and facilitate appropriate functioning of intra-abdominal organs [21]. Previous reports have shown that the marked contractile ability in SPFs was implicated in the colonic strictures in Crohn's disease [22,23]. In the field of peritoneal dialysis, SPFs have been reported to produce growth factors, cytokines, or chemokines in response to TGF-β stimulation and have been implicated in the failure of peritoneal dialysis [24]. However, the implication of SPFs in tumor progression is not known, and our study is the first to report the contribution of SPFs in tumor progression and metastasis that is dependent on peritoneal invasion in colon cancer.

Our findings seem to support the concept of microenvironmental regulation of cancer. The tumor microenvironment consists of distinct cell types, including fibroblasts, blood cells, vascular-originated cells, and more. They synergistically create a distinct microenvironment according to tumor progression, such as the core primary tumor microenvironment, the invasive tumor microenvironment, or the metastatic tumor microenvironment [9]. Area-specific tissue microarrays were very useful to expand this concept into the pathological phenomenon and biological study was then performed based on these results. Interestingly, the fibroblasts we obtained from the submucosal and subperitoneal tissues showed biological differences dependent on the histoanatomical site. In addition, our finding of marked phenotypical modification in SPFs suggests that fibroblasts from different histoanatomical sites show different reactions to cancer stimuli. We used Caco-2 with low tumorigenic and metastatic potential and DLD-1 with a higher tumorigenic and metastatic potential in this study. DLD-1 has been known to preferentially cause lymph node metastasis rather than lung or liver metastasis, and our data is in accordance with previous reports [25–28]. Together with the xenograft tumor results in which SPFs enhanced tumor growth and tumor formation in Caco-2 and DLD-1, and promote lymph node metastasis in DLD-1, we have clarified that this fibroblastic difference is implicated in colon cancer progression that is dependent on peritoneal invasion.

In general, fibroblasts within the tumor stroma, so-called CAFs, acquired a modified phenotype. CAFs are enriched in α-SMA positive active myofibroblasts and are known to play an active role in tumor progression [29,30]. Residual fibroblasts are one of the sources of CAFs, and residual fibroblasts exposed to cancer stimulation show phenotypical modification. Although the tumor-promoting ability of CAFs has been reported to be diverse and dependent on cancer origin, intra-tumoral diversity has not been clear [31]. Our data suggests the physiological diversity of fibroblasts within one organ produces the intra-tumoral diversity of CAFs. Therefore, gene profiles in fibroblasts with and without cancer CCCM stimulation may provide new insights into their diversity in colon cancer.

We are speculating that a fibroblast subpopulation with tumor-promoting capacity can be enriched in the subperitoneal layer. Their original phenotype may include a previously reported CAFs marker, and variable gene modification in response to cancer stimuli could be a characteristic feature of tumor-promoting fibroblasts. Recently, activated proteins in CAFs have been considered to be a target of therapy [32]. However, not all kinds of CAFs may promote tumor progression [31]. Our gene expression profile data in SPFs with and without CCCM stimulation may also be useful for future stromal-target therapy. SPFs with robust tumor promotion ability showed higher gene expression associated with an ECM component, and marked gene upregulation associated with cell contraction, including α-SMA, after CCCM stimulation. Recently both stromal-cell contractile ability and ECM stiffness have been reported to influence epithelial cell migration and invasion. Also, α-SMA is one of the representative markers of CAFs and myofibroblasts, and its expression is associated with biological contractile ability. Furthermore, α-SMA expression in tumor stroma was reported to be a prognostic factor in colorectal cancer. Therefore, our result suggests the importance of mechanotransduction theory in the study of the tumor microenvironment [33–35].

From the first categorization efforts reported by Lockhart-Mummery, primary colon cancer has been consistently stratified based on the extent of its spread into the bowel wall [36]. More recent pathological investigations have revealed that peritoneal invasion is a prognostic factor, and is a candidate for discriminating high-risk stage II colon cancer, and those patients who may receive benefit from post-operative therapy [3,37,38]. We and others reported the utility of elastica stain for the objective diagnosis of peritoneal invasion. We have proven that objective identification of peritoneal invasion is also useful for investigating biological phenomena specifically occurring in this tumor microenvironment [39]. Recently, Liang et al. proposed that pT3 tumors with ELI should be subdivided into further categories like pT3b [6]. Our findings support the subdivision of cases with ELI from those without ELI, and the diversity of the fibroblasts could be one factor associated with frequent metastases in cases with ELI.

In conclusion, fibrosis with α-SMA expression is a significant feature of the cancer microenvironment formed by peritoneal invasion in human colon cancer. The biological features and functions of fibroblasts in the subperitoneal tissue are different from those in submucosal tissue, and their phenotypical modification by cancer stimuli and contribution to tumor growth and metastasis are also different. Specifically, SPFs from the subperitoneal tissue showed characteristic biological features of a marked ECM component and contractile-associated gene expression, and functions that accelerate tumor formation and metastasis. Considering these comprehensive pathological and biological data, we propose that CMPI is a special microenvironment that promotes tumor growth and metastasis. In CMPI, SPFs and cancer cells interaction play an active and crucial role in tumor progression.

Supporting Information

Figure S1 Biological characteristics of subperitoneal fibroblasts and submucosal fibroblasts. (A) Immunocytochemical staining for vimentin in SPFs. (B) Immunocytochemical staining for vimentin in SMFs. (C) Flow cytometric analysis of SPFs and SMFs. (D) Immunocytochemical staining of SPFs and SMFs. Protein expression results were positive for vimentin and CD105, and negative for an epithelial marker (AE1/3), a neural marker (S-100), mesothelial markers (calretinin, CK8), endothelial markers (CD31, 34), and lymphocyte and monocyte markers (CD3, 14, 20, 45, 68), suggesting that the obtained cells were fibroblasts. We found weak α-SMA expression in a few SPFs and SMFs. (E) Growth curve of SPFs (blue) and SMFs (red). SPFs showed significantly longer doubling time than did SMFs ($P<0.01$). Results are presented as the mean ± SE of triplicate measurements ($^{**}P<0.01$).
(TIF)

Figure S2 Morphometric analysis of immunocytochemical α-SMA expression. α-SMA expression was upregulated specifically and significantly in SPFs after cancer-cell-conditioned medium (CCCM) stimulation. Results are presented as the mean ± SE of 3 experiments ($^{*}P<0.05$).
(TIF)

Table S1 Patient Characteristics Entered into Area-Specific Tissue Microarray.
(DOCX)

Table S2 Primary antibodies used in this study.
(DOCX)

Table S3 Upregulated gene clusters and composing genes in SPFs compared with SMFs.
(DOCX)

Table S4 Top 20 genes in SPFs compared with SMFs.
(DOCX)

Table S5 Upregulated gene clusters in SPFs with cancer-cell-conditioned medium (CCCM) stimulation compared with SMFs with CCCM stimulation.
(DOCX)

Table S6 Top 20 upregulated genes in SPFs with cancer cell-conditioned medium (CCCM) stimulation compared with SMFs with CCCM stimulation.
(DOCX)

Materials and Methods S1 Supplementary Materials and Methods.
(DOCX)

Acknowledgments

We thank MA's Communications Inc. for their excellent English editing support.

Author Contributions

Conceived and designed the experiments: MK YH GI AO. Performed the experiments: MK YH AO. Analyzed the data: MK YH KA HS. Contributed reagents/materials/analysis tools: MY NS. Wrote the paper: MK YH AO.

References

1. Sobin LH, Gospodarowicz MK, Wittekind CH (2009) TNM Classification of Malignant Tumors, (7th edn), New York: Wiley-Blackwell, Inc. 15 p.
2. Newland RC, Dent OF, Lyttle MN, Bokey L (1994) Pathologic determinants of survival associated with colorectal cancer with lymph node metastases. A multivariate analysis of 579 patients. Cancer 73: 2076–2082.
3. Shepherd NA, Baxter KJ, Love SB (1997) The prognostic importance of peritoneal involvement in colonic cancer: a prospective evaluation. Gastroenterology 112: 1096–1102.
4. Stewart CJ, Morris M, de Boer B, Iacopetta B (2007) Identification of serosal invasion and extramural venous invasion on review of Dukes' stage B colonic carcinomas and correlation with survival. Histopathology 51: 372–378.
5. Kojima M, Nakajima K, Ishii G, Saito N, Ochiai A (2010) Peritoneal elastic laminal invasion of colorectal cancer: the diagnostic utility and clinicopathologic relationship. Am J Surg Pathol 34: 1351–1360.
6. Liang WY, Zhang WJ, Hsu CY, Arnason T, Berger D, et al. (2013) Retrospective Evaluation of Elastic Stain in the Assessment of Serosal Invasion of pT3N0 Colorectal Cancers. Am J Surg Pathol "in press".
7. Shinto E, Ueno H, Hashiguchi Y, Hase K, Tsuda H, et al. (2004) The subserosal elastic lamina: an anatomic landmark for stratifying pT3 colorectal cancer. Dis Colon Rectum 47: 467–473.
8. Shinto E, Tsuda H, Ueno H, Hashiguchi Y, Hase K, et al. (2005) Prognostic implication of laminin-5 gamma 2 chain expression in the invasive front of colorectal cancers, disclosed by area-specific four-point tissue microarrays. Lab Invest 85: 257–266.
9. Hanahan D, Weinberg RA (2011) Hallmarks of cancer: the next generation. Cell 144: 646–674.
10. Sobin LH, Wittekind CH (1997) TNM Classification of Malignant Tumors, (5th edn), New York: Wiley-Liss.
11. Tsujino T, Seshimo I, Yamamoto H, Ngan CY, Ezumi K, et al. (2007) Stromal myofibroblasts predict disease recurrence for colorectal cancer. Clin Cancer Res 13: 2082–2090.
12. Witowski J, Jorres A (2006) Peritoneal cell culture: fibroblasts. Perit Dial Int 26: 292–299.
13. Hoshino A, Ishii G, Ito T, Aoyagi K, Ohtaki Y, et al. (2011) Podoplanin-positive fibroblasts enhance lung adenocarcinoma tumor formation: podoplanin in fibroblast functions for tumor progression. Cancer Res 71: 4769–4779.
14. Huang DW, Sherman BT, Lempicki RA (2009) Systematic and integrative analysis of large gene list using DAVID bioinformatics resources. Nat Protoc 4: 44–57.

15. Huang DW, Sherman BT, Lempicki RA (2009) Bioinformatics enrichment tools: paths toward the comprehensive functional analysis of large gene lists. Nucleic Acids Res 37: 1–13.
16. Fukushima N, Kikuchi Y, Nishiyama T, Kudo A, Fukayama M (2008) Periostin deposition in the stroma of invasive and intraductal neoplasms of the pancreas. Mod Pathol 21: 1044–1053.
17. Bae YK, Kim A, Kim MK, Choi JE, Kang SH et al. (2013) Fibronectin expression in carcinoma cells correlates with tumor aggressiveness and poor clinical outcome in patients with invasive breast cancer. Hum Pathol "in press".
18. Maximow AA, Bloom W (1942). Textbook of Histology. 4th edition ed. Philadelphia: W. B. Saunders Company: 54–75.
19. Kaye GI, Lane N, Pascal RR (1968). Colonic pericryptal fibroblast sheath: replication, migration, and cytodifferentiation of a mesenchymal cell system in adult tissue. II. Fine structural aspects of normal rabbit and human colon. Gastroenterology 54: 852–865.
20. Nik AM, Reyahi A, Ponten F, Carlsson P (2013) Foxf2 in intestinal fibroblasts reduces numbers of Lgr5(+) stem cells and adenoma formation by inhibiting Wnt signaling. Gastroenterology 144: 1001–1011.
21. van der Wal JB, Jeekel J (2007) Biology of the peritoneum in normal homeostasis and after surgical trauma. Colorectal Dis 9 Suppl 2: 9–13.
22. Brannigan AE, Watson RW, Beddy D, Hurley H, Fitzpatrick JM (2002) Increased adhesion molecule expression in serosal fibroblasts isolated from patients with inflammatory bowel disease is secondary to inflammation. Ann Surg 235: 507–511.
23. Regan MC, Flavin BM, Fitzpatrick JM, O'Connell PR (2000) Stricture formation in Crohn's disease: the role of intestinal fibroblasts. Ann Surg 231: 46–50.
24. Witowski J, Thiel A, Dechend R, Dunkel K, Fouquet N (2001) Synthesis of C-X-C and C-C chemokines by human peritoneal fibroblasts: induction by macrophage-derived cytokines. Am J Pathol 158: 1441–1450.
25. Oikonomou E, Kothonidis K, Zografos G, Nasioulas G, Andrea L et al. (2007) Newly established tumorigenic primary human colon cancer cell lines are sensitive to TRAIL-induced apoptosis in vitro and in vivo. Br J Cancer 97: 73–84.
26. Kawada K, Hosogi H, Sonoshita M, Sakashita H, Manabe T et al. (2007) Chemokine receptor CXCR3 promotes colon cancer metastasis to lymph nodes. Oncogene 26: 4679–4688.
27. Céspedes MV, Espina C, Gracia-Cabezas MA, Trias M, Boluda A et al. (2007) Orthotopic microinjection of human colon cancer cells in nude mice induces tumor foci in all clinically relevant metastatic sites. Am J Pathol 170: 1077–1085.
28. de Vries JE, Dinjens WN, De Bruyne GK, Verspaget HW, van der Linden EP et al. (1995) In vivo and in vitro invasion in relation to phenotypic characteristics of human colorectal carcinoma cells. Br J Cancer 71: 271–277.
29. Polanska UM, Orimo A (2013) Carcinoma-associated fibroblasts: Non-neoplastic tumour-promoting mesenchymal cells. J Cell Physiol 2013; 228: 1651–1657.
30. Kalluri R, Zeisberg M (2006) Fibroblasts in cancer. Nat Rev Cancer 6: 392–401.
31. Erez N, Truitt M, Olson P, Arron ST, Hanahan D (2010) Cancer-associated fibroblasts are activated in in cipient neoplasia to orchestrate tumor promoting inflammation in an NF-kappaB-dependent manner. Cancer Cell 17: 135–147.
32. Brennen WN, Isaacs JT, Denmeade SR (2012) Rationale behind targeting fibroblast activation protein-expressing carcinoma-associated fibroblasts as a novel chemotherapeutic strategy. Mol Cancer Ther 11: 257–66.
33. Levental KR, Yu H, Lakins JN, Egeblad M, Erler JT, et al. (2009) Matrix crosslinking forces tumor progression by enhancing integrin signaling. Cell 139: 891–906.
34. Butcher DT, Alliston T, Weaver VM (2009) A tense situation: forcing tumor progression. Nat Rev Cancer 9: 108–122.
35. Kümper S, Marshall CJ (2011) ROCK-driven actomyosin contractility induces tissue stiffness and tumor growth. Cancer Cell 19: 695–697.
36. Lockhart-Mummery JP (1926) Two hundred cases of cancer of the rectum treated by perineal excision. British Journal of Surgery 14: 110–124.
37. Newland RC, Chapuis PH, Smyth EJ (1987) The prognostic value of substaging colorectal carcinoma. A prospective study of 1117 cases with standardized pathology. Cancer 60: 852–857.
38. Dotan E, Cohen SJ (2011) Challenges in the management of stage II colon cancer. Semin Oncol 38: 511–520.
39. Kojima M, Yokota M, Saito N, Nomura S, Ochiai A (2012) Elastic laminal invasion in colon cancer: diagnostic utility and histological features. Front Oncol "in press".

OPEN ACCESS

Pathological diagnostic criterion of blood and lymphatic vessel invasion in colorectal cancer: a framework for developing an objective pathological diagnostic system using the Delphi method, from the Pathology Working Group of the Japanese Society for Cancer of the Colon and Rectum

Motohiro Kojima,[1] Hideyuki Shimazaki,[2] Keiichi Iwaya,[2] Masayoshi Kage,[3] Jun Akiba,[4] Yasuo Ohkura,[5] Shinichiro Horiguchi,[6] Kohei Shomori,[7] Ryoji Kushima,[8] Yoichi Ajioka,[9] Shogo Nomura,[10] Atsushi Ochiai[1]

▶ Additional material is published online only. To view please visit the journal online (http://dx.doi.org/10.1136/jclinpath-2012-201076).

For numbered affiliations see end of article.

Correspondence to
Dr Atsushi Ochiai, Pathology Division, Research Center for Innovative Oncology, National Cancer Center Hospital East, 6-5-1 Kashiwanoha, Kashiwa, Chiba 277-8577, Japan; aochiai@east.ncc.go.jp

Received 20 July 2012
Revised 25 December 2012
Accepted 8 January 2013
Published Online First
16 April 2013

▶ http://dx.doi.org/10.1136/jclinpath-2013-201587

To cite: Kojima M, Shimazaki H, Iwaya K, *et al*. *J Clin Pathol* 2013;**66**:551–558.

ABSTRACT

Aims The goal of this study is to create an objective pathological diagnostic system for blood and lymphatic vessel invasion (BLI).

Methods 1450 surgically resected colorectal cancer specimens from eight hospitals were reviewed. Our first step was to compare the current practice of pathology assessment among eight hospitals. Then, H&E stained slides with or without histochemical/immunohistochemical staining were assessed by eight pathologists and concordance of BLI diagnosis was checked. In addition, histological findings associated with BLI having good concordance were reviewed. Based on these results, framework for developing diagnostic criterion was developed, using the Delphi method. The new criterion was evaluated using 40 colorectal cancer specimens.

Results Frequency of BLI diagnoses, number of blocks obtained and stained for assessment of BLI varied among eight hospitals. Concordance was low for BLI diagnosis and was not any better when histochemical/immunohistochemical staining was provided. All histological findings associated with BLI from H&E staining were poor in agreement. However, observation of elastica-stained internal elastic membrane covering more than half of the circumference surrounding the tumour cluster as well as the presence of D2-40-stained endothelial cells covering more than half of the circumference surrounding the tumour cluster showed high concordance. Based on this observation, we developed a framework for pathological diagnostic criterion, using the Delphi method. This criterion was found to be useful in improving concordance of BLI diagnosis.

Conclusions A framework for pathological diagnostic criterion was developed by reviewing concordance and using the Delphi method. The criterion developed may serve as the basis for creating a standardised procedure for pathological diagnosis.

INTRODUCTION

Blood and lymphatic vessel invasion (BLI) in colorectal cancer (CRC) are known to be strong risk factors correlated with poor outcome. Since it was first reported by Brown *et al* in 1938, numerous studies have been conducted on BLI. BLI is adopted in TNM Classification of Malignant Tumours and College of American Pathologists Consensus Statement in pathology reports.[1–4] Assessment of BLI enables identifying patients with high risk within the same TNM stage and therapeutic strategy can be tailored accordingly, especially for patients with Stage II CRC and patients with endoscopically resected pT1.[5–7] Observation of BLI, however, is also known for its weakness, which is high interobserver variability. Many articles report poor interobserver concordance of BLI assessment and no solution has been offered so far.[8–10] One solution may be to use elastica for histochemical staining or D2-40 for immunohistochemical staining of internal elastic lamina of vessel and lymphatic endothelium.[11–15] Another solution may be to take a conventional approach to develop a framework for diagnostic criterion, through formal procedure to reach consensus, gain support and understanding of pathologists worldwide.[16] It was under this concept that pathologists belonging to the Japanese Society for Cancer of the Colon and Rectum decided to join hands and took a comprehensive approach as follows: (1) review current practice of pathologists' assessment including sampling methods, staining methods and BLI in different medical institutions (2) evaluate concordance of BLI diagnosis and histological findings associated with BLI (3) develop a framework for diagnostic criterion using the Delphi method, with data from current practice and (4) conduct a concordance study to evaluate the usefulness of the new criterion. Our attempt was to develop a framework for an objective criterion to assess BLI, in order to improve concordance in all settings.

MATERIALS AND METHODS

Multicentre, retrospective review of pathological assessment at different departments of pathology

A total of 1450 patients with CRC who underwent surgical resection in 2003 from eight institutions under the Japanese Society for Cancer of the Colon and Rectum were reviewed. Clinicopathological factors including the TNM stage according to the

fifth edition of TNM classification,[3] the presence of BLI, number of paraffin blocks taken to examine primary tumours, use of mega-block, tangential tissue sectioning, histochemical staining and immunohistochemical staining were reviewed and compared.[17] The range of histochemical staining and antibody used for immunohistochemical staining were also reviewed.

Interobserver study

Eighty consecutive, surgically resected specimens of Stage II CRC according to the seventh edition of TNM classification[4] between 2003 and 2005 from the National Cancer Center Hospital East were used for the interobserver study. Eight pathologists from eight institutions assessed the slides. Specimens for pathological assessment were divided into six cohorts as follows (table 1) and concordance of diagnosis was reviewed. Cohort 1: H&E-stained slides without any guiding criteria. Cohort 2: H&E-stained slides without any criteria, but focus on designated area of lesion. Assessment was later checked to see which histological findings associated with BLI had good agreement. Concordance of assessment for designated area was also reviewed (figure 1). Cohort 3: H&E-stained, elastica-stained and D2-40-stained slides. Histochemical and immunohistochemical staining without any guiding criteria. Cohort 4: H&E-stained, elastica-stained and D2-40-stained slides. Histochemical and immunohistochemical staining without any guiding criteria but focus on designated area of lesion (figure 1). Observation was later checked to determine which slides of H&E, histochemical or immunohistochemical staining associated with BLI diagnosis had good concordance. Concordance of assessment for designated area of lesion was also reviewed. Cohort 5: H&E-stained, elastic-stained and D2-40-stained slides. Histochemical and immunohistochemical staining and our new criterion were used for assessment. Finally, for Cohort 6, the same H&E-stained, elastic-stained and D2-40-stained slides used in Cohort 3 were assessed by the pathologists (who were unaware of reviewing the same slides) to check diagnostic agreement of histochemical and immunohistochemical staining using our new criterion. Cohorts 1, 3, 5 and 6 each consisted of 20 CRC specimens and Cohorts 2 and 4 each consisted of 10 CRC specimens. H&E-stained slides and slides of largest slice from blocks of specimen including the deepest invasive area of tumour were used in Cohorts 1, 3, 5 and 6, while one representative slide of the tumour was used in Cohorts 2 and 4. In Cohorts 2 and 4, assessment of designated area was reviewed to evaluate the agreement of BLI diagnosis. Three areas of lesion containing histological tumour cluster surrounded by some space or fibrous rim-like vascular structure were chosen randomly and marked with ink. Since the designated area was very small, virtual slides were used to indicate with an arrow where assessment should be made (figure 1). In Cohorts 1, 3, 5 and 6 the 'presence' or 'absence' of BLI was reported. In Cohorts 2 and 4, assessment of designated area was made as 'blood vessel invasion', 'lymphatic vessel invasion' or 'neither'. In Cohorts 2 and 4, histological findings associated with the diagnosis of BLI were collected. This was reviewed thoroughly in a meeting and was recorded in the survey sheet, as either 'present' or 'absent' (table 2).

Developing diagnostic criteria using the Delphi method

Four rounds of consensus meetings, participated by eight pathologists were held as shown in figure 2. Before the meeting, a survey on histological, histochemical and immunohistochemical diagnostic criteria of BLI was prepared. All pathologists were requested to answer the survey anonymously and send it by mail after the meeting.[16] There were a total of 34 questions: 2 on the definition of BLI, 7 on the assessment of BLI, 4 on the use of histochemical and immunohistochemical staining, 8 on assessment of blood vessel invasion and 13 on the assessment of lymphatic vessel invasion (table 3). Scoring was based on 1 to 6 Likert scale (1=strong disagreement, 2=moderate disagreement, 3=some disagreement, 4=some agreement, 5=moderate agreement, 6=strong agreement), maximum score being 6 points. Scores of 5 and 6 were regarded as 'agreement'. Consensus was considered to be achieved when over 80% of the participants' scores resulted in 'agreement', based on the previously described scoring method.[18–20] Four rounds of meetings with active discussion took place and surveys were conducted three times, after the second and third rounds of meetings, as shown in figure 2. At the beginning of the second and third rounds of meetings, interim results of survey were reported to the

Table 1 Details of cohorts and concordance of blood and lymphatic vessel invasion (BLI)

H&E staining	D2-40 and elastica staining	Designated area of lesion	Criterion		κ Value	95% CI	Positive ratio (%)
Cohort 1							
+	−	−	−	Agreement in blood vessel invasion	0.524	0.441 to 0.606	28.1
+	−	−	−	Agreement in lymphatic vessel invasion	0.216	0.133 to 0.299	32.5
Cohort 2							
+	−	+	−	Agreement in BLI	0.466		
Cohort 3							
+	+	−	−	Agreement in blood vessel invasion	0.502	0.419 to 0.584	73.8
+	+	−	−	Agreement in lymphatic vessel invasion	0.153	0.071 to 0.236	33.8
Cohort 4							
+	+	+	−	Agreement in BLI	0.622		
Cohort 5							
+	+	−	+	Agreement in blood vessel invasion	0.547	0.464 to 0.630	42.5
+	+	−	+	Agreement in lymphatic vessel invasion	0.492	0.409 to 0.575	26.9
Cohort 6							
+	+	−	+	Agreement in blood vessel invasion	0.617	0.534 to 0.700	75.6
+	+	−	+	Agreement in lymphatic vessel invasion	0.618	0.534 to 0.700	31.9

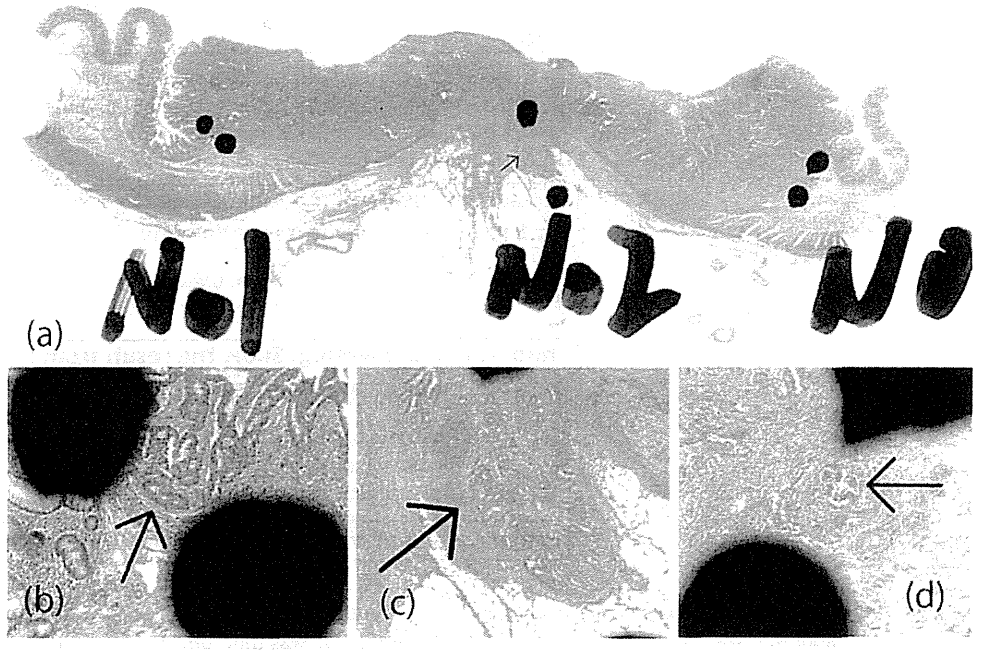

Figure 1 (A–D) A case from Cohort 2. In Cohorts 2, 4, three regions of interest within the histological tumour cluster with surrounding space or fibrous rim-like vascular structure were chosen randomly and marked with ink near the lesion (A). The lesion to be reviewed was indicated with an arrow on the virtual slides (B–D). Eight pathologists reviewed the slides. The assessment for each of the indicated lesions was reported as 'blood vessel invasion', 'lymphatic vessel invasion' or 'neither'. Furthermore, pathological findings associated with the diagnosis of blood and lymphatic vessel invasion were studied. Reviewers recorded their interpretations of the indicated lesion using the query sheet, answering the questions as 'present' or 'absent'.

participants to facilitate building consensus on key histological findings with high concordance. For findings that failed to present immediate agreement, further discussion took place and the next vote was performed. Consistent with the Delphi method, some questions in the survey were modified to enable building general agreement.[18] After the third round of meetings, the findings for which consensus had been reached were summarised and new diagnostic criterion was developed.

Statistical analysis

The concordance reached by pathologists on rating tumour invasion was evaluated using κ coefficients. Using %mκ SAS macro, we

Table 2 Concordance of histological findings associated with the blood and lymphatic vessel invasion

Histological findings	κ Value	95% CI
Cohort 2		
Presence of space around tumour nests	0.492	0.424 to 0.560
Presence of endothelium around tumour nests	0.518	0.451 to 0.586
Presence of vascular smooth muscle around tumour nests	0.412	0.344 to 0.479
Presence of spicula at the periphery of tumour nests	0.308	0.240 to 0.376
Presence of lymphatic fluid in peritumoural space	0.454	0.386 to 0.522
Presence of blood cells in peritumoural space	0.395	0.327 to 0.462
Difficult to distinguish blood and lymphatic vessel	0.064	−0.033 to 0.132
Presence of continuity in normal blood or lymphatic vessel	0.276	0.209 to 0.344
Cohort 4		
Presence of space around tumour nests	0.471	0.404 to 0.539
Presence of endothelium around tumour nests	0.269	0.201 to 0.336
Presence of vascular smooth muscle around tumour nests	0.372	0.305 to 0.440
Presence of spicula at the periphery of tumour nests	0.002	−0.066 to 0.069
Presence of lymphatic fluid in peritumoural space	0.142	0.075 to 0.210
Presence of blood cells in peritumoural space	0.055	−0.013 to 0.122
Difficult to distinguish blood and lymphatic vessel	0.055	−0.013 to 0.123
Presence of continuity in normal blood or lymphatic vessel	0.150	0.082 to 0.217
Growth along with normal artery	0.491	0.424 to 0.559
Presence of elastica-stained internal elastic membrane covering more than half of the circumference surrounding the tumour cluster	0.801	0.734 to 0.869
Presence of D2-40 positive cells covering more than half of the circumference surrounding the tumour cluster	0.451	0.383 to 0.518
Presence of D2-40 positive endothelial cells covering more than half of the circumference surrounding the tumour cluster	0.682	0.615 to 0.750

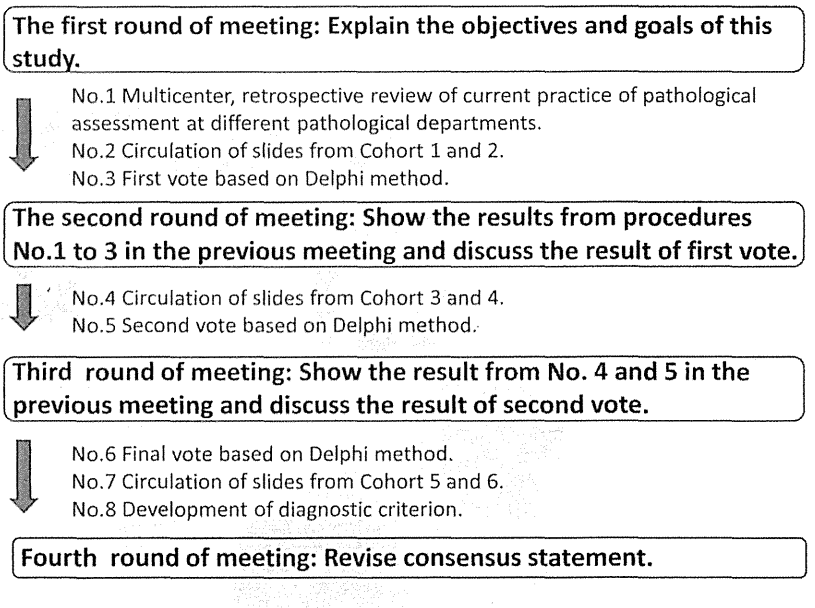

Figure 2 Time flow for consensus development.

estimated the Fleiss type multi-rater κ coefficient and corresponding 95% CI.[21] All statistical analyses was performed with SAS Release V.9.3 (SAS Institute, Inc, Cary, North Carolina, USA).

RESULTS

Multicentre retrospective review of current practice of pathological assessments

The result of the study is shown in table 4 and figure 3. The total number of cases reviewed in this study by eight institutions ranged from 54 to 441, of which 51.0–72.5% were colon cancer, 53.5–68.0% were male patients, and their average age was between 63 years and 68 years. The average number of paraffin blocks used for primary tumour pathological assessment varied widely among institutions, ranging from 4.8 blocks to 34.4 blocks. Use of histochemical staining and immunostaining was also different among eight institutions. And the range of histochemical staining performed was also different. Antibody used in immunohistochemical staining was D2-40 in three institutions. And one institution used D2-40 and alpha-smooth muscle actin (SMA). Figure 3 shows the results of a retrospective review of the stage and assessment of BLI. Although the stage distributions were similar among the eight institutions (Stage 0, I; 19.8–28.0%, Stage II; 10.2–17.4%, Stage III; 12.1–21.5% and Stage IV; 3.0–9.9%), substantial difference was noted on the presence of BLI (lymphatic vessel invasion; 18.9–74.8%, blood vessel invasion; 17.7–66.7%). None of the institutions in this study used megablock or tangential sectioning.

Interobserver study and development of diagnostic criterion using the Delphi method

The result of the interobserver study is shown in table 1. After the first round of meeting, Cohorts 1 and 2 were given only H&E stained slides without any additional staining or guiding criteria. The concordance of assessment of blood vessel invasion was moderate and it was low for lymphatic vessel invasion. This was not any better when pathologists in Cohort 2 were asked to focus on the designated area. Furthermore, the concordance of all histological findings associated with BLI was low in Cohort 2 (table 2). Diagnosis of BLI is based on multiple histological findings considered to be associated with BLI, most of which were included in this study as shown in table 2. Consistent diagnosis of BLI only with H&E-stained slides seemed to be difficult to achieve and this was informed to the pathologists during the second round of meetings. It was then decided to distribute H&E-stained slides as well as the histochemical and immunohistochemical staining, without any guiding criteria (Cohorts 3 and 4). Although this increased positive findings of blood vessel invasion in Cohort 3, it did not improve the concordance of BLI diagnosis. In Cohort 4, concordance improved for the designated area. Interestingly, we found few histochemical and immunohistochemical findings associated with the diagnosis of BLI having good agreement (table 2). This was reported to pathologists during the third round of meetings and it was agreed that they should be included in the diagnostic criteria of BLI (table 3). Pathologists summarised the findings which they were able to agree upon and new diagnostic criterion was developed with active discussion (box 1). Finally, the use of the new criterion was evaluated with Cohorts 5 and 6. There was a remarkable improvement in concordance in Cohort 5 (κ=0.547 for blood vessel invasion, κ=0.492 for lymphatic vessel invasion), as well as in Cohort 6 (κ=0.617 for blood vessel invasion, κ=0.618 for lymphatic vessel invasion), which used the same slide as in Cohort 3 (κ=0.502 for blood vessel invasion, κ=0.153 for lymphatic vessel invasion). This serves as direct evidence on the usefulness of new criterion in improving agreement in BLI diagnosis (table 1).

DISCUSSION

The need for a diagnostic criterion which enables a standardised and objective diagnosis is clear. Our attempt was to provide a framework for developing a consensus-based criterion to be used in different pathological settings through this study. BLI are distinct pathological factors and have different clinicopathological implications.[22] There are, however, some common morphologies such as the presence of endothelium or cavity, and distinct identification of small venules and lymphatic vessel is often difficult. There is also the problem of interobserver variability.[2] BLIs are strong risk factors in many types of cancer. In CRC, BLIs can be used as a criterion to determine the need for adjuvant therapy in Stage II cases, which account for a significant proportion of CRC cases (27.1% in this study). For endscopically resected pT1 cases, BLIs are reported to be risk factors of lymph node metastasis and can be used as a criterion for making a decision of surgical resection. In this study, we tried to solve interobserver variabilities in BLI. The criterion that we developed may be useful for achieving